공학석사 학위논문

Numerical Simulation of Structure Phase Change under High Heat Flux Condition Coupled with Nuclear System Analysis Code

고열속 조건 시 구조재 상변화 열전달 모사를 위한
원자로 계통 열수력 코드 연계 수치해석 연구

2019년 8월

서울대학교 대학원
에너지시스템공학부
최 희 수

Numerical Simulation of Structure Phase Change under High Heat Flux Condition Coupled with Nuclear System Analysis Code

고열속 조건 시 구조재 상변화 열전달 모사를 위한 원자로 계통 열수력 코드 연계 수치해석 연구

지도교수 조 형 규

이 논문을 공학석사 학위논문으로 제출함
2019 년 7 월

서울대학교 대학원
에너지시스템공학부
최 희 수

최희수의 석사 학위논문을 인준함
2019 년 7월

위 원 장	이 유 호	(인)
부위원장	조 형 규	(인)
위 원	권 성 진	(인)

Abstract

Numerical Simulation of Structure Phase Change under High Heat Flux Condition Coupled with Nuclear System Analysis Code

Hee Su Choe
Department of Energy System Engineering
The Graduate School
Seoul National University

Under the high heat flux transient conditions that can occur in a nuclear system, the thermal and structural integrity of several structures can be worsened. In particular, because of the high temperature plasma and its instabilities, high heat flux conditions can easily apply to the plasma facing components in a nuclear fusion reactor. It causes the phase change of the material, such as melting and evaporation of structure. Furthermore, the temperature increase due to the applied high heat flux may cause a burnout situation in the cooling channel, so that the heat transfer efficiency can be drastically reduced. The phase change of structure affects the heat transfer phenomenon in both solid material and cooling system connected to it. Thus, the thermal-hydraulic analysis for the phase change behavior of the structure and the two-phase flow heat transfer in the cooling system are necessary for the safety analysis. Studies on the safety so far, however, have been limited to segregated calculations for a structure phase change or a

system analysis. Therefore, the main objective of this study is to simulate the phase change in structures by a code coupling with a nuclear system thermal-hydraulic analysis code.

First, for the simulation of heat transfer including the phase change through the wall, the one-dimensional phase change calculation module with evaporation and melting model was developed. The limitations due to the imaginary concept of mushy zone used in the effective heat capacity method, the melting model, were identified. To improve it, a mesh adaptation technique using a monitoring function was adopted in the module. The technique reconstructs the mesh at each time step, according to the temperature profile in the structural material. As a result, the calculation efficiency and utilization of the calculation module were improved. With the improvements in the numerical module, calculation time was reduced by 5 times and it facilitates a more realistic melting simulation. After the improvement, the one-dimensional phase change simulation module was coupled with MARS-KS using its DLL version. Its purpose was to analyze the cooling system with the coupled code between the solid phase change and thermal-hydraulic behavior.

Afterwards, the phase change simulation was conducted for the first wall of blanket, one of the plasma facing structures in a nuclear fusion demonstration reactor, K-DEMO. The VDE scenario caused by plasma instability was analyzed in 5 cases classified by the heat flux size and the transient duration time. For these cases, evaporation and melting thickness, penetration depth, and the duration of phase change time were compared with each other.

In addition, the two-dimensional melting calculation was conducted using ANSYS-FLUENT to identify the natural convection effects that could occur inside of the melted layer. As a result, the internal flow of the structure made a slight shape change of the solid–melt interface. The coupled calculation between ANSYS-FLUENT and MARS-KS was progressed as well. CORBA was used as a

program-to-program control method and both socket communication and file input/output method were used for code coupling. According to the established code coupling methodology, the transient phenomenon under high heat flux condition on the blanket was simulated and the occurrence of film boiling in the coolant channel was observed. Following the transition to the film boiling, it was also identified that reduced cooling performance and increased melting duration time.

……...

Keywords: high heat flux transient analysis, solid phase change heat transfer, mushy zone, mesh adaptation technique, blanket, MARS, FLUENT

Student Number: 2017-27568

List of Contents

List of Tables

List of Figures

Chapter 1.

Introduction

1.1 Background

Proper control of heat is required in various fields using high temperature condition such as a nuclear power plant, or a nuclear fusion reactor. The safety analysis of nuclear power plant has been performed in various countries for decades. In addition, as the researches on the conceptual design of nuclear fusion demonstration plant have been progressed, the necessity of safety study based on the accident scenario in the DEMO reactors increases. Recently, the thermal behavior of the structure under sudden transient including phase change of materials in a nuclear system becomes one of the major study issues. For example, under abnormal high power conditions, the centerline of fuel can locally melt (Welland et al., 2008). In addition, the melting of the pressure vessel wall can be driven by in-vessel corium retention during a severe accident (Park et al., 2017). In the nuclear fusion reactors, there exist plasma facing components (PFCs) such as divertor or blanket that can be easily exposed to a high heat flux by a plasma instability or disruption and damaged by erosion (Hassanein, 2008).

The accident scenarios in the water-cooled fusion reactors were proposed by Nakamura (2014). For the initiators, LOFA (loss of coolant flow in the cooling system), LOCA (loss of coolant of the cooling system), a local increase in the heat

load, and the transient thermal energy release due to the disruption were described. In the previous studies, the temperature of components reaches a melting temperature after several seconds (Hong et al., 2018, Komen et al., 1994). Therefore, both structure thermal behavior simulation including its phase change and the thermal-hydraulic calculation of the whole system are required for safety analysis in nuclear reactors.

Although researches on both structural phase change and system thermal-hydraulic phenomenon are essential, it has not been done sufficiently. The coupled simulation between different codes is necessary because of the features and the limitations of conventional methods. There exist some codes that can be used for transient analysis. First, the nuclear system analysis code such as MARS-KS (Multidimensional Analysis of Reactor Safety) and RELAP5 (Reactor Excursion and Leak Analysis Program) are efficient for simulating thermal-hydraulic phenomenon in nuclear systems. However, those codes cannot simulate phase change of structural materials due to a lack of melting and evaporation models. In this respect, the one-dimensional phase change calculation module that can be coupled with system analysis code was developed by Kim (2017). In addition, in general cases, the structural phase change is accompanied with multi-dimensional effects in real. A CFD code can simulate melting and evaporation of structure in two- or three-dimensions. But it is inefficient to analyze the whole system with the CFD code.

In this study, for the plasma facing component in K-DEMO, numerical simulation and CFD calculation were conducted for thermal behavior analysis. In order to consider the thermal-hydraulic behavior of the system together, nuclear system analysis code MARS-KS was coupled with the calculation module or

ANSYS-FLUENT. The schematic design for K-DEMO and its plasma facing components are illustrated in Figure 1.1.

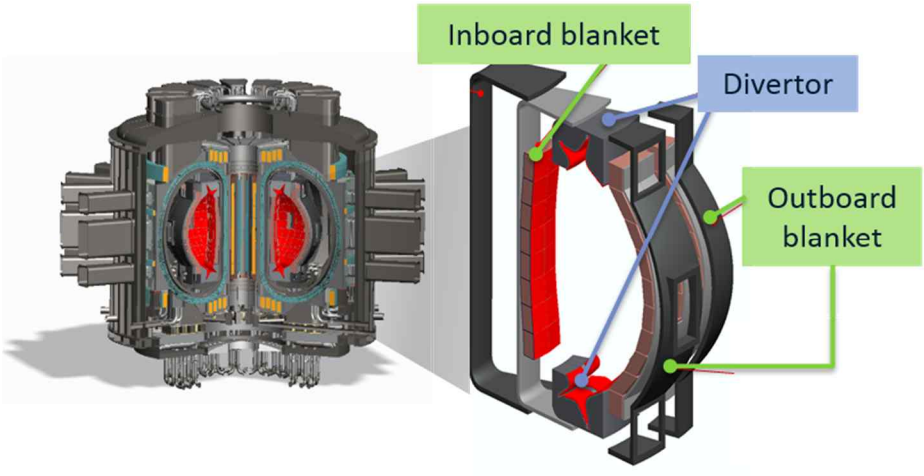

Figure 1.1 K-DEMO design (Kim et al., 2015)

1.2 Objective and scope

In the purpose of effective melting and evaporation simulation for structure in the nuclear system, numerical models in the one-dimensional phase change calculation module were reviewed. Afterwards, a numerical method to improve the computational performance of the phase change simulation was implemented to the module in this study.

Meanwhile, a convective flow in a melted layer can change the shape of the liquid-vapor or liquid-solid surface (Kohei et al., 2018, Beckermann et al., 1988). In order to identify the effect of the natural convection in a melted layer and simulate the multi-dimensional phase change simulation under high heat flux condition, the methodology of code coupling between CFD code ANSYS-FLUENT and the system analysis code MARS-KS was developed.

The remainder of the thesis is divided into four main sections. In Chapter 2, the numerical models for the solid phase change are reviewed. Those models were implemented into the one-dimensional structure phase change simulation module, and the module was improved with the mesh adaptation technique. In Chapter 3, the transient scenarios under the high heat flux in fusion reactors are introduced, and one-dimensional phase change simulation under various conditions coupled with MARS-KS was conducted with a developed numerical module. Chapter 4 deals with the simulation of the multi-dimensional structural phase change. The methodology of the code coupling between ANSYS-FLUENT and MARS-KS was developed. The coupled code simulated structural phase change for identifying the effect of natural convection in the melting of structure. Finally, concluding remarks are given in Chapter 5.

Chapter 2.

Development of 1-D Phase Change Simulation Module

2.1 Literature review on the numerical phase change simulation model

The one-dimensional phase change simulation module solves the heat conduction equation with considering material evaporation and melting at the structural wall surface where high heat flux is induced. In this section, the literature review on the numerical phase change simulation models and their implementation will follow.

2.1.1 Evaporation model

A numerical model to evaluate the amount of the material evaporation for the plasma disruption events was proposed by Hassanein (1984) based on the energy partitioning boundary condition at the vapor-melt interface. On the surface of the heat influx, the total heat flux of plasma disruption $F(t)$ imposed to the wall can be partitioned into three different heat transfer mechanisms as

$$F(t) = -k_l(T_v)\frac{\partial T_l(s)}{\partial x} + \rho_l(T_v)L_v v(t) + \varepsilon\sigma(T_v^4 - T_0^4) \tag{2.1}$$

where,

T_v : surface temperature (K)

T_0 : temperature of the first wall surface not exposed to the plasma directly but in direct line of sight of the exposed surface (K)

T_l : liquid temperature (K)

L_v : latent heat of vaporization (J/mol)

k_l : thermal conductivity of the liquid wall (W/m·K)

ε : emissivity of the surface material

σ : Stefan-Boltzmann constant of the surface material

$v(t)$: receding velocity of the surface (m/s)

Based on the Hertz-Knudsen-Langmuir theory often used to correlate the evaporation data, the time rate of change of the gas molecules concentration on the surface can be expressed as a function of the pressure of the gas. However, the theory is not adoptable to the intense evaporation. If the surface temperature rises due to the high heat flux during the plasma disruption in a tokamak reactor, the vapor expands into a vacuum rapidly so that the condensation is negligible. That is the reason why the rate of evaporation J_e^{eq} was defined using saturated vapor pressure P_s in vacuum vessel as seen below;

$$P_s = P_0 \exp(-L_v / kT) \tag{2.2}$$

$$J_e^{eq} = \frac{P_s}{\sqrt{2m\pi kT_v}} \tag{2.3}$$

where,

P_0 : constant based on the Clausius-Clapeyton relation

k : Boltzmann constant

During the intense evaporation in the surface, the re-condensation of the vapor appears through the collision mechanism. After expands to a vacuum, evaporated atoms can collide with each other in the following frequency τ_c. Then the vapor atoms backscattered and condensed into the surface.

$$\frac{1}{\tau_c} = 16\sqrt{2}\pi^{1/3}\left(\frac{3}{4}\Omega\right)^{2/3} J_e^{eq} \tag{2.4}$$

where, Ω : atomic volume (cm^3)

The evaporation model proposed by Hassanein (1984) deals with both evaporation and condensation mechanisms as mentioned before. Therefore, the velocity of the receding surface can be expressed as a function of the saturated pressure of the gas, temperature of the surface, and the collision frequency τ_C related to the atomic volume as follows;

$$v(t) = \Omega J_e^{eq}[0.8 + 0.2\exp(-t/10\tau_C)] \tag{2.5}$$

The evaporation model mentioned above was implemented into the one-dimensional phase change simulation module. The code-to-code verification was

completed in the previous study (Kim et al., 2017) by reproducing the benchmark problem results. The problem defined as stainless steel evaporation under several plasma disruption cases as shown in Figure 2.1. Figure 2.2 (a) and (b) show the results of code-to-code verification.

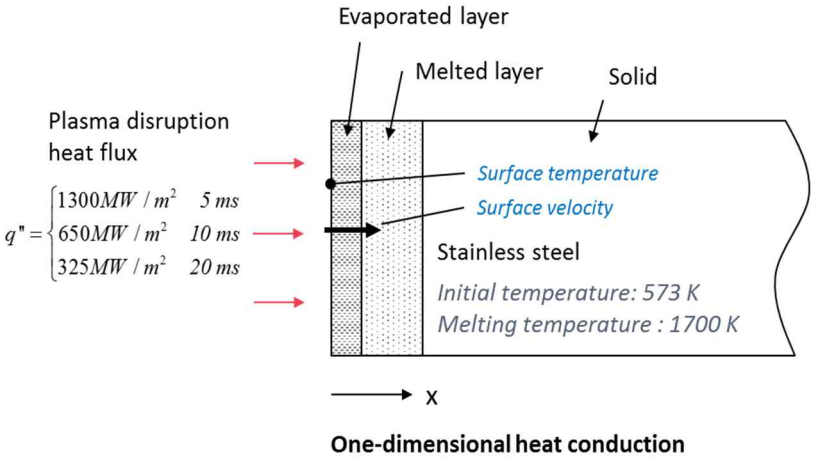

Figure 2.1 Benchmark problem of evaporation simulation (Kim et al., 2017)

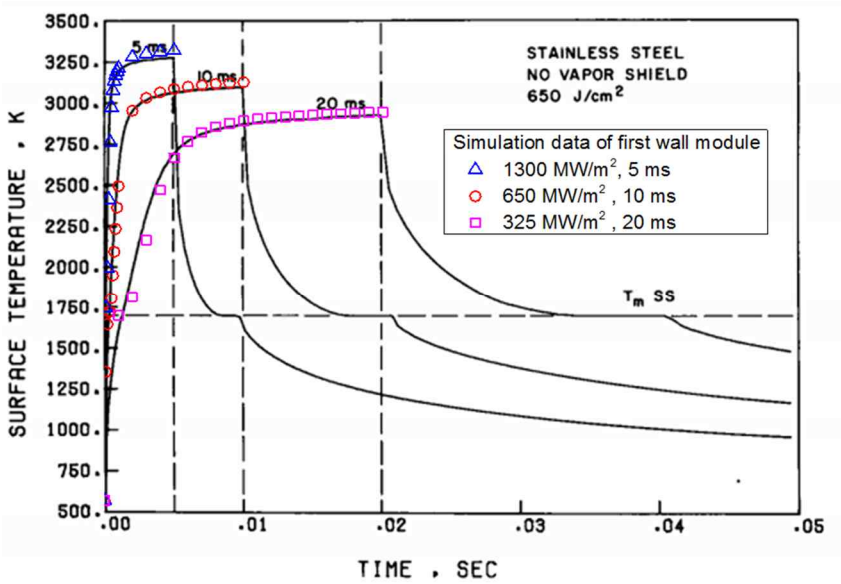

(a) Surface temperature rise of stainless steel

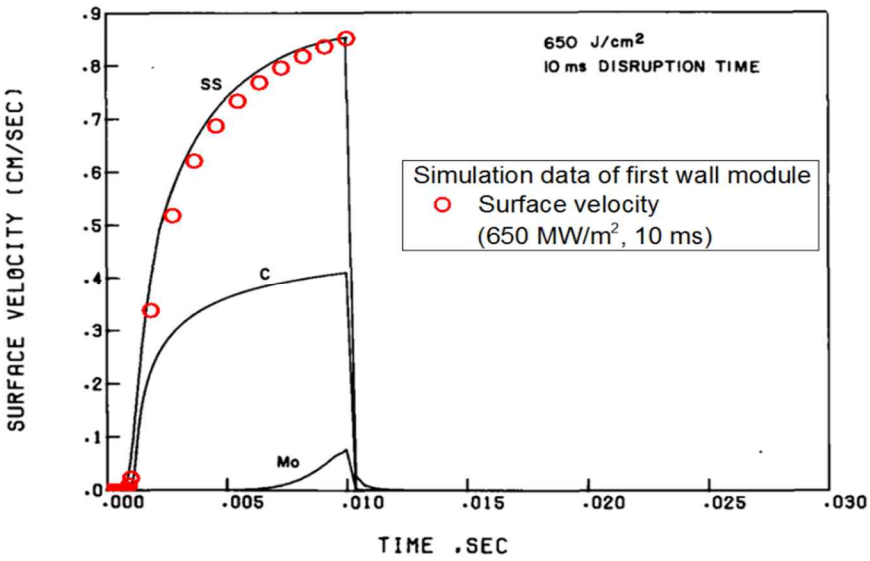

(b) Surface velocity of stainless steel

Figure 2.2 Comparison result of benchmark problem of stainless steel evaporation : one-dimensional module by Kim (2017) vs. Hassanein (1984)

2.1.2 Melting model: Effective heat capacity method

In general, the phase change processes in the single-component phase change materials (PCM) occur at its melting point. In contrast, for a multi-component PCM, a process of the solid and liquid phase change occurs over a range of temperatures; this is called the mushy zone. Figure 2.3 shows the temperature rise in a melting process of a single and multi-component, and the temperature range from T_{m1} to T_{m2} is defined as a mushy zone. As shown in the right part of Figure 2.3, the mushy zone appears between a solid-liquid interface in a multi-component PCM, while the solid-liquid interface in a single component PCM appears as a sharp border. However, the numerical melting model requires a virtual concept of temperature range, where melting and re-solidification occur even for a single component PCM in order to consider the latent heat in the melting process calculation.

A numerical model, effective heat capacity method (EHCM), was adopted to simulate the melting phenomena in the first wall. Figure 2.4 is the conceptual diagram of EHCM. The model adjusts the heat capacity (C_p) of the heat conduction equation (2.6) by defining effective heat capacity ($C_{p,eff}$) in the mushy zone as a function of temperature below.

$$\rho C_p \frac{\partial T}{\partial t} = \nabla \cdot k \nabla T + Q \tag{2.6}$$

$$C_{p,eff}(T) = L / \Delta T_{mushy} + C_p(T)$$
$$\text{where} \quad T_m - \frac{\Delta T_{mushy}}{2} \le T \le T_m + \frac{\Delta T_{mushy}}{2} \tag{2.7}$$

where,

T_m : melting temperature of the material (K)

T : temperature at a position (K)

C_p : heat capacity at a position (J/kg·K)

L : specific latent heat of melting (J/kg)

ΔT_{mushy} : temperature range of mushy zone (K)

k : thermal conductivity (W/m·K)

ρ : density (kg/m^3)

The specific latent heat of melting is considered as a local increase of the heat capacity in a mushy zone of the PCM as shown in Figure 2.4. The Verification of the melting model implemented in the one-dimensional phase change simulation module was conducted following Stefan's problem (Ogoh & Groulx, 2010) of paraffin wax depicted in Figure 2.5. The analytic solution of Stefan's problem is determined as follows (Ozisik, 1968),

$$T(x,t) = T_w - (T_m - T_w)\frac{erf(x/2\sqrt{\alpha t})}{erf(\beta)} \tag{2.8}$$

where,

$$\beta e^{\beta^2} erf(\beta) = \frac{C_p(T_w - T_m)}{L\sqrt{\pi}}$$

$$\alpha = \frac{k}{\rho C_p}$$

$$\beta = \frac{\delta(t)}{2\sqrt{\alpha t}}$$

Figure 2.6 and 2.7 show the verification results through the temperature profile in a PCM and the position of the melted depth. Figure 2.8 shows the calculation results and the effect of mushy zone size on the same Stefan's problem presented above. As shown in the figure, the results of melting simulation are affected by the size of the mushy zone, which does not exist for a single component PCM and arbitrarily selected in the numerical process. In other words, the adopted melting model, EHCM has some limitations due to the imaginary concept of mushy zone. The mushy zone size as small as possible, which reflects the sharp solid-liquid interface is desired in order to reduce the distortion of the real phenomenon. However, small mushy zone size leads to a non-converged simulation result. Accordingly, a very small time step and the computational meshes are required in order to capture the consumed specific latent heat during an abrupt melting process and to achieve convergence. Otherwise, the heat transfer to the wall cannot be correctly simulated, because the melting front propagates into the wall, passing over some cells in the domain. It makes over-prediction of the material temperature and melted depth. Consequently, the selection of a mushy zone size takes into account the following conditions. The temperature of the material at any position should not exceed the mushy zone within one time step. And the mesh size in the mushy zone should be small enough to accurately calculate the latent heat.

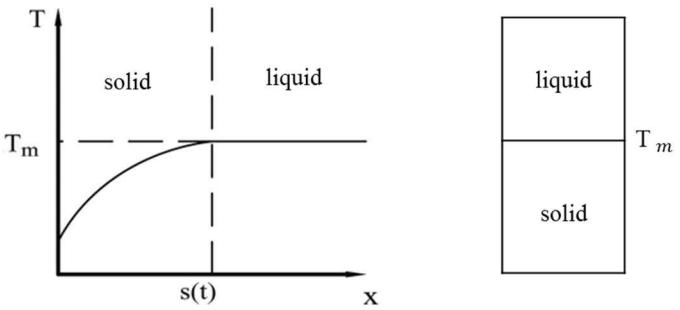

<Single-component PCM>

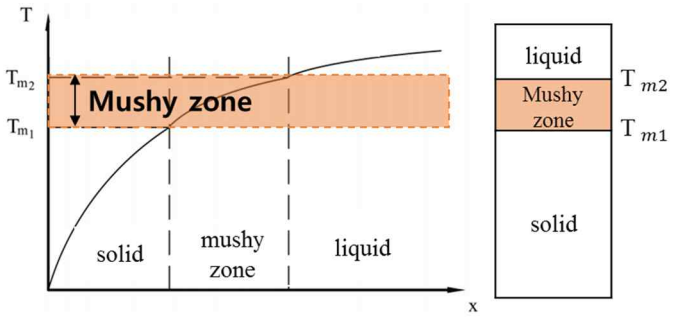

<Multi-component PCM>

Figure 2.3 Temperature in melting process (left) and PCM phase (right)

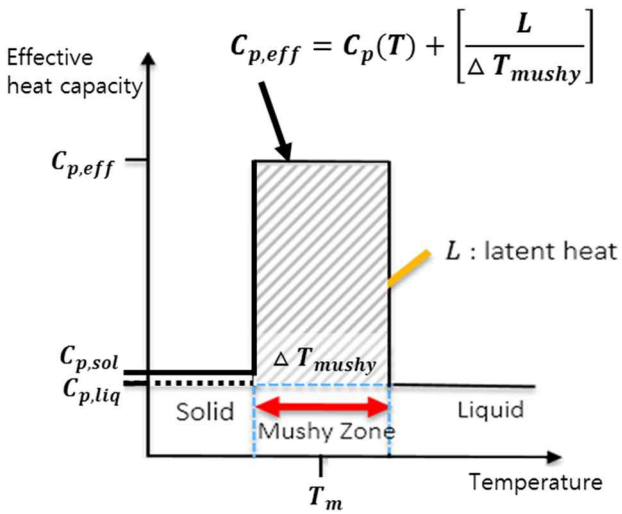

Figure 2.4 Conceptual diagram of effective heat capacity method

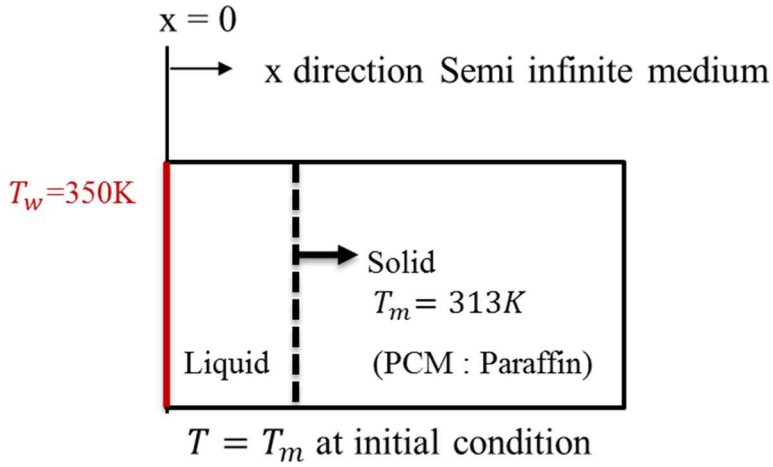

Figure 2.5 Stefan problem definition: paraffin wax as PCM

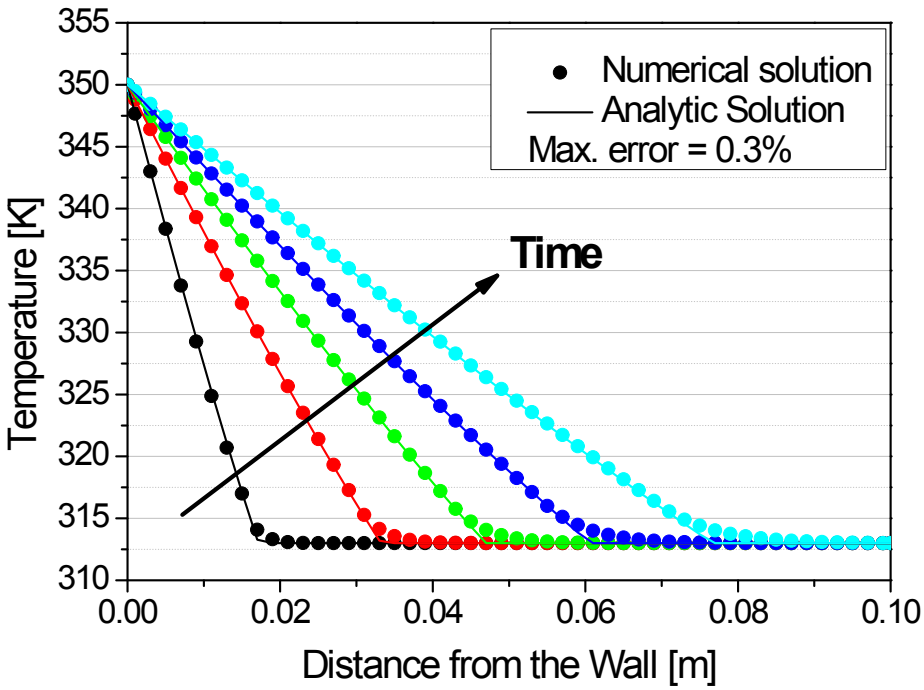

Figure 2.6 Temperature distribution in paraffin wax

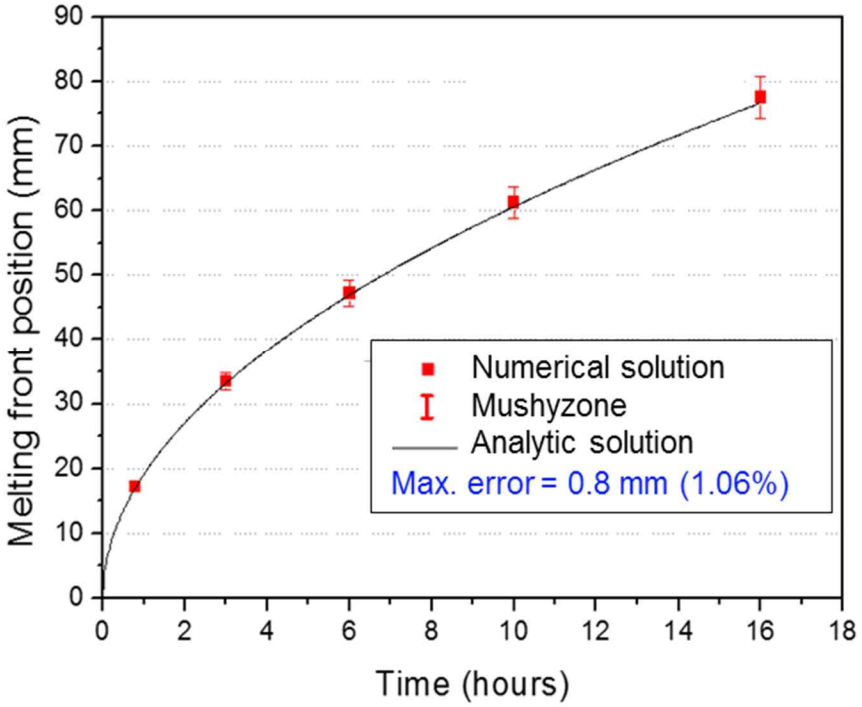

Figure 2.7 Melting front position in paraffin wax

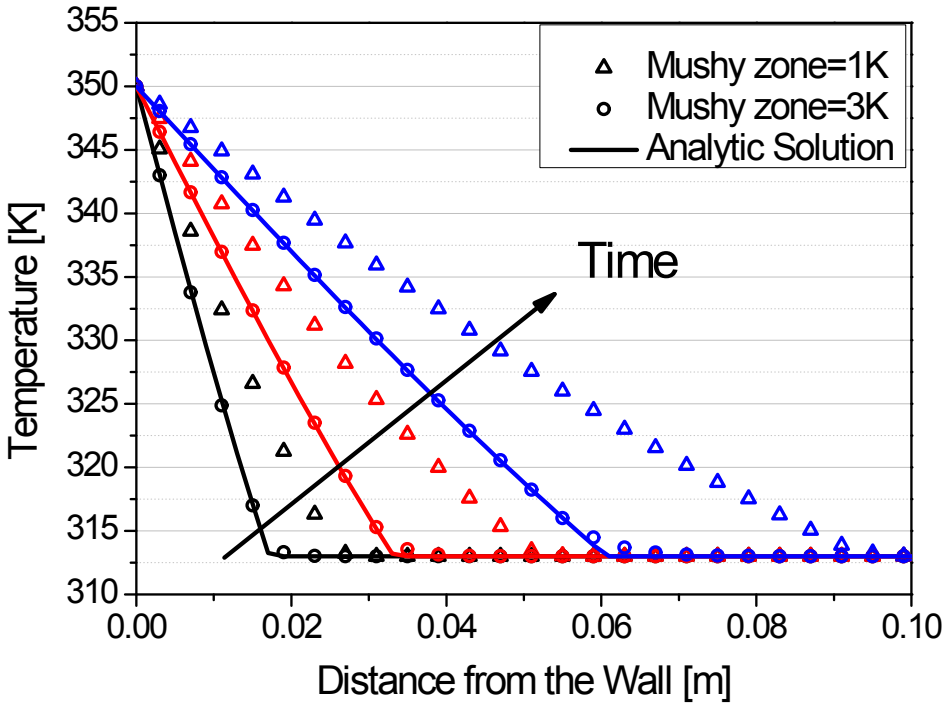

Figure 2.8 Effect of mushy zone size

2.2 Improvement of phase change module

According to the limitation of EHCM mentioned in the previous section, very fine structural mesh is required in the mushy zone region where the phase change occurs, because of the abrupt changes in the value of heat capacity and other properties. However, the computational domain of a single-phase part where the heat conduction equation is solved with continuous properties can achieve converged solutions with relatively large mesh size. Therefore, if the whole computational domain has a small uniform mesh, it has the limitation of increasing the unnecessary calculation cost. Additionally, a fixed stretched mesh system cannot be applied to the whole domain in the transient simulations because the melting front propagates into the depth direction of the wall during simulation time. These limitations of EHCM become the motivation to apply a mesh adaptation technique in the module.

2.2.1 Mesh adaptation technique in the PCM structure

There exist two typical approaches to performing the mesh adaptation process, the h-refinement and r-refinement methods. Figure 2.9 is the schematic diagram of the two different methods. The h-refinement method coarsens or refines a mesh locally in the interested part by varying the total number of the cells in the whole calculation domain. It usually makes the change in the size of the calculating matrix. On the other hand, the r-refinement method, which is called moving mesh methods redistributes a fixed number of cell nodes, concentrating a higher density of cells in interested regions. In order to achieve small meshes in the mushy zone region for the convergence of the melting simulation, the mesh adaptation

technique with r-refinement method was implemented in the one-dimensional phase change simulation module. The technique continues to track the position of a mushy zone near the melting temperature and generates relatively denser meshes locally in the mushy zone than those in the other parts. The sequence of mesh adaptation technique is as follows.

Monitoring Function

First of all, the mesh adaptation technique starts by using a monitoring function for the melting front, where the material temperature reaches the melting point. At each time step, the monitoring function m is defined as,

$$m = \frac{1}{1 + \frac{|T(x,t) - T_m|}{\Delta T_{mushy}}} \tag{2.9}$$

The shape of this function and its corresponding mushy zone are depicted in Figure 2.10 (a). It has the maximum value at the x-position where the temperature reaches the melting point T_m. As the cell temperature approaches the melting point, function m abruptly increases through the mushy zone while it increases gradually in the rest of the region. The rapid increase of the monitoring function at the mushy zone becomes the basis of the mesh adaptation technique.

Accumulative Function

At each time step, the accumulative integration function $\alpha(x,t)$ of the monitoring function along x-position can be calculated as below:

$$\alpha(x,t) = \int m(x,t)dx \tag{2.10}$$

Figure 2.10 (b) is the enlarged view of an accumulative integration function of monitoring function represented in Figure 2.10 (a). As shown in Figure 2.10 (b), the accumulative integration function rapidly increases and it has a steep slope at the melting point. At the same time, the total cumulative integral value $\alpha_0(t)$ is defined as;

$$\alpha_0(t) = \int_a^b m(x,t)dx \tag{2.11}$$

The notation a and b refer to the both end positions of the materials in x-direction such as depth of the first wall in the blanket. In the phase change simulation module which will be described in Chapter 3, each notation a and b represents the position of the plasma facing surface and the other end of the first wall coordinates, respectively.

Mesh redistribution with equi-distribution principle

Finally, with the defined monitoring function and its integral function, the mesh adaptation technique is conducted by adopting equi-distribution principle (Ong, 2013; Nochetto, 2009). A fixed number of meshes are reconstructed to equally divide the accumulative integral function $\alpha(x,t)$. In other words, the re-distributed grids are obtained to satisfy the following equation.

$$\int_{x_{j-1}}^{x_j} m(x,t)dx = \frac{\alpha_0(t)}{N} \tag{2.12}$$

x_{j-1}, x_j, and N refers to the coordinate of the new grid points in depth direction obtained from the mesh adaptation technique, and the total number of meshes in the calculating domain.

At this time, the r-refinement method is used in mesh adaptation technique. Straight lines in Figure 2.10 (b) indicates the final step of mesh adaptation. The values of an accumulative function marked in the vertical axis are equally distributed, and the x-positions of new grids are calculated back to the horizontal axis. Accordingly, the re-distributed meshes concentrated in the mushy zone.

Figure 2.11 shows the mesh adaptation results in a particular time. A graph on the top indicates the temperature distribution on the PCM material, tungsten. At the 0.4 mm in depth direction, the temperature reaches the melting point 3673 K. The monitoring function shows the maximum value at the same position. The graph in the bottom shows the final result of the redistributed mesh size. The mesh size at the melting point and mushy zone region decreases to the 2.5 % smaller than the maximum mesh.

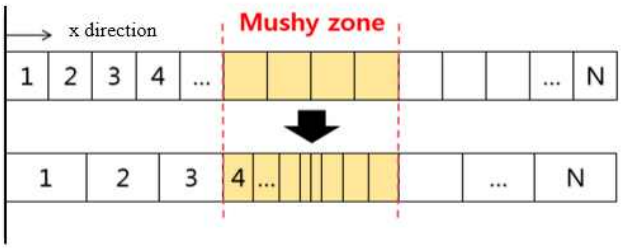

(a) r-refinement method

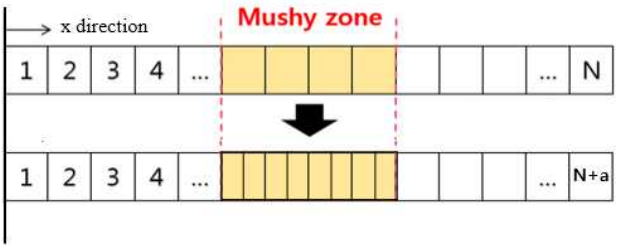

(b) h-refinement method

Figure 2.9 Mesh refinement methods

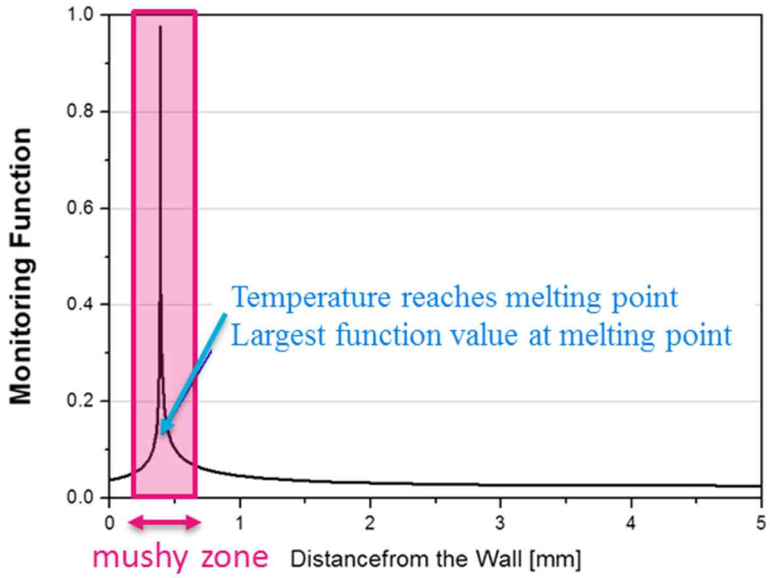

(a) Example of monitoring function 'm'

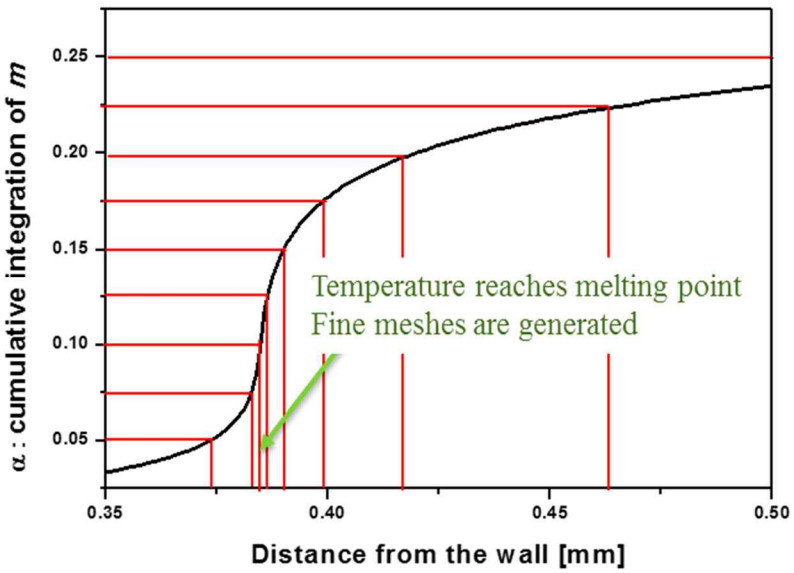

(b) Enlarged example of accumulative integration 'α' and equi-distribution

Figure 2.10 Examples of monitoring function and its accumulative integration

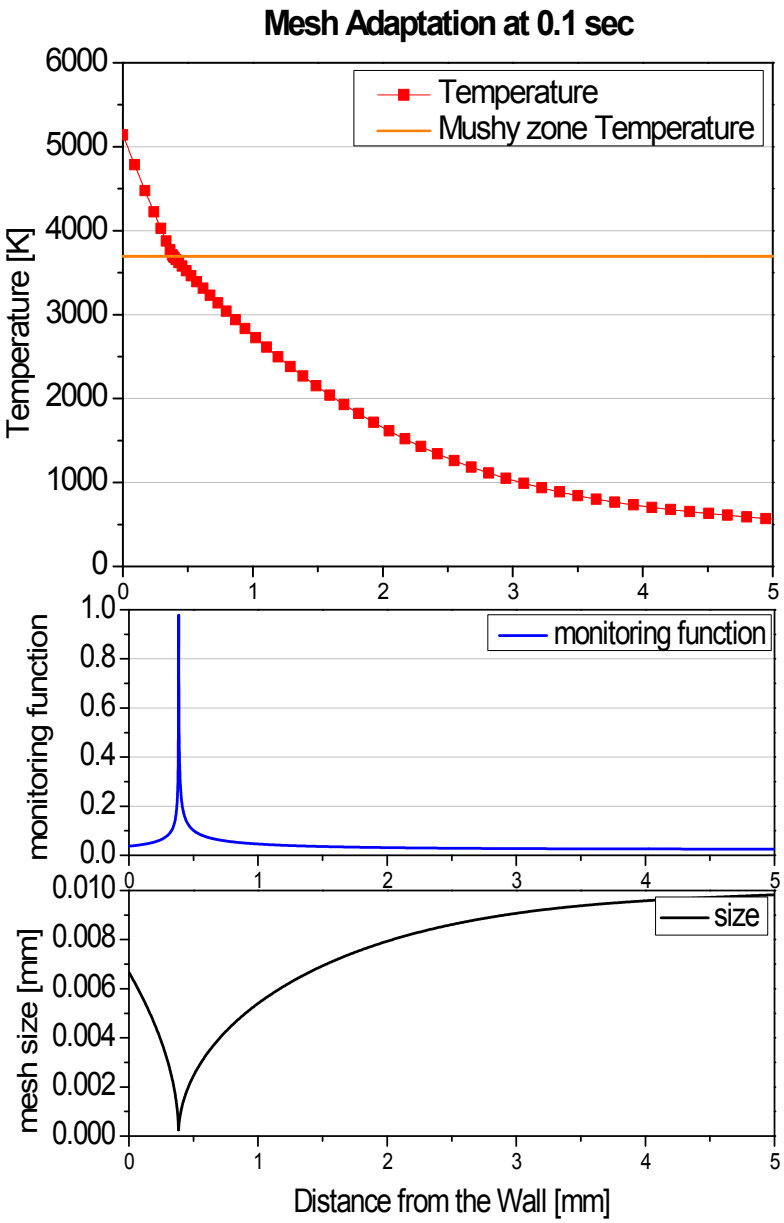

Figure 2.11 Mesh adaptation result at typical time (t = 0.1 sec)
Temperature (Top), monitoring function (Center), re-meshed cell size (Bottom)

2.2.2 Mesh reconstruction in vapor-melt interface

The second issue in the mesh reconstruction is induced from the evaporated thickness. In the previous study (Kim, 2017), the uniform reconstruction method was used in the vapor to melt interface reconstruction. After the mesh adaptation process proposed in section 2.2.1 in this study, the reconstruction method was modified to partly uniform reconstruction type. This method redistributes the nearest grids close to the surface except for far ones. The difference between those two methods is shown in Figure. 2.12.

At the early stage of the phase change process, the melting point is located near the vapor-melt interface. However, due to the penetration of the melting front into the material, the redistributed meshes near the vapor-melt surface become larger. In order to retain the accurate temperature data at the vapor-melt interface, the upper limit of the surface mesh size is adopted as 130% compared to the base mesh size.

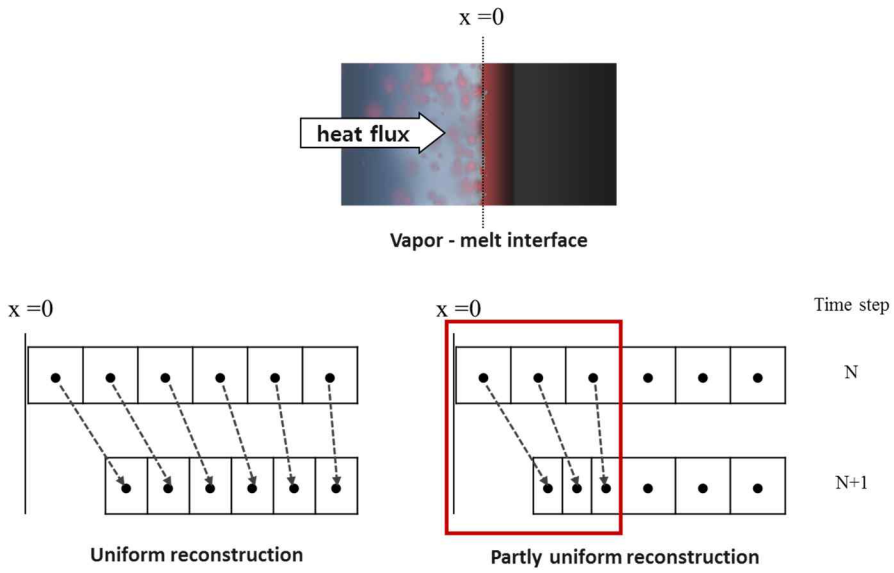

Figure 2.12 Vapor-melt interface and reconstruction methods

2.2.3 Implementation of the mesh adaptation technique in the calculation module

This sequence of mesh adaptation technique was implemented into the one-dimensional phase change simulation module to capture the melting front and the receding surface due to evaporation with an affordable fixed number of meshes. The whole algorithm for the phase change simulation in the one-dimensional calculation module is shown in Figure. 2.13.

Before the melting process starts, the module solves the heat conduction equation with a melting model, EHCM for uniformly distributed meshes. If the surface temperature, which is initially the maximum temperature of the material, reaches the melting point, mesh adaptation starts. At first, the velocity of the receding surface is calculated with the evaporation model. The heat conduction equation with the EHCM is solved under uniformly distributed mesh system. Then, through the mesh adaptation sequence using a monitoring function and the equi-distribution principle depending on the calculated temperature, relatively fine meshes are generated in the mushy zone. After that, a partly uniform reconstruction of the vapor-melt surface is conducted. Next, the temperatures of the previous time step at re-distributed meshes are second-order interpolated with the neighboring cells. Finally, the temperature at the present step is re-calculated by solving a heat conduction equation once again involving EHCM under new meshes. The whole sequence of the algorithm is repeated, until the end of the simulation. The code verification was performed for the improved module with Stefan's problem described in section 2.1.

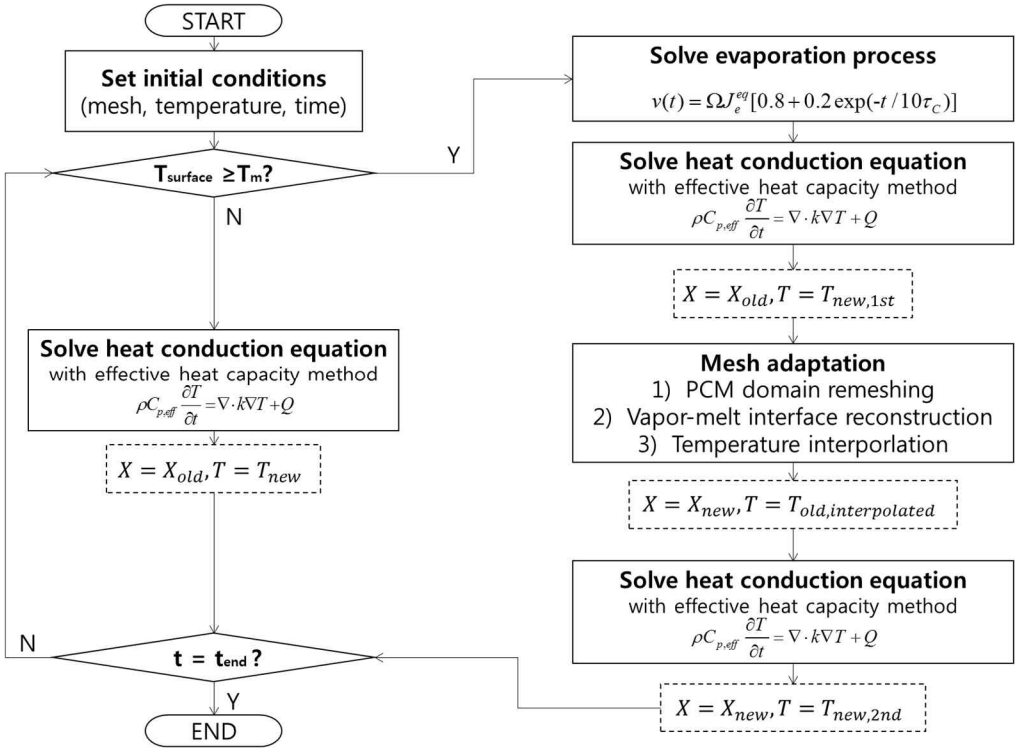

Figure 2.13 Algorithm of one-dimensional phase change calculation

Chapter 3.

Phase Change Simulation with 1-D In-house Module coupled with MARS-KS

3.1 Phase change simulation under various high heat flux conditions

The melting and evaporation simulation was progressed under the high heat flux transient scenario in a tokamak reactor. The transient scenario was selected to VDE (Vertical Displacement Event) in a water-cooled tokamak reactor. The target structure was an outboard blanket sector OB module, which is one of the plasma facing components in K-DEMO. As shown in Figure 3.1, the target module is located near the bottom divertor and tilted by 45.6° in the radial direction. The size, materials, and location of the target first wall module are illustrated in Figure 3.1. The coolant channels for the target are depicted in the same figure.

In this section, the thermal integrity test involving structure phase change simulation was conducted by the one-dimensional phase change simulation module developed and improved in Chapter 2. The mesh adaptation was applied only to the first layer, the tungsten part. At the same time, a nuclear reactor safety analysis code, MARS-KS was coupled with the module and it calculated the heat transfer between a target structure and the flow in the cooling channels.

3.1.1 Vertical Displacement Event in a tokamak reactor

The VDE is defined as the uncontrolled plasma motion in a vertical direction that induces high heat flux to the surrounding structures in a tokamak reactor, such as K-DEMO. High heat flux from the VDE can degrade the integrity of the structures by imposing thermal energy deep into the components. For the transient analysis of the VDE cases, it was assumed that the energy of the whole plasma is entirely transferred to the first wall of a single blanket module without current reducing. In addition, the heat flux to the blanket module was assumed uniform along with the toroidal and poloidal directions. Due to the lack of detail data on the thermal loads of the VDE in the K-DEMO plasma, the boundary condition of the high heat flux imposed on the blanket module was obtained from the simulation data according to the ITER. According to Cardella (2000), the energy load to the blanket is 60 MJ/m^2 in the ITER. In the present study, the simulation conditions were subdivided into five different cases varying the VDE duration time and the heat flux boundary conditions as listed in Table 3.1. The whole energy imposed on the first wall is equal to 60 MJ/m^2 in every case, while case number I (VDE-I) lasting for 0.1 second with the highest heat flux 600 MW/ m^2 and the case number V (VDE-V) lasting for 0.3 second with smaller heat flux.

To be more specific on the problem conditions, the mesh adaptation technique was adopted only in the tungsten layer, 5 mm depth from the plasma facing surface, and the other layers, 1 mm vanadium and 0.5 mm RAFM were calculated in uniformly distributed meshes with 50 μm size. The size of the mushy zone selected for the melting simulation and the number of meshes in the tungsten layer vary in a range as listed in Table 3.1. The effect of mushy zone size, grid sensitivity tests will be discussed in the next section 3.1.3 to 3.2.

Table 3.1 Problem definition

Cases	I	II	III	IV	V
Time conditions [sec]					
VDE duration time	0.1	0.15	0.2	0.25	0.3
Time step size in normal operation	0.1 sec				
Time step size in transient condition	0.0001 sec				
Boundary conditions – heat flux [MW/m^2]					
Normal operation	0.455				
VDE	600	400	300	240	200
After VDE	0				
Modeling conditions					
Mushy zone range	1 ~ 10 K				
Mesh number (W)	100 ~ 5000				
Mesh size (V/ RAFM)	50 μm				

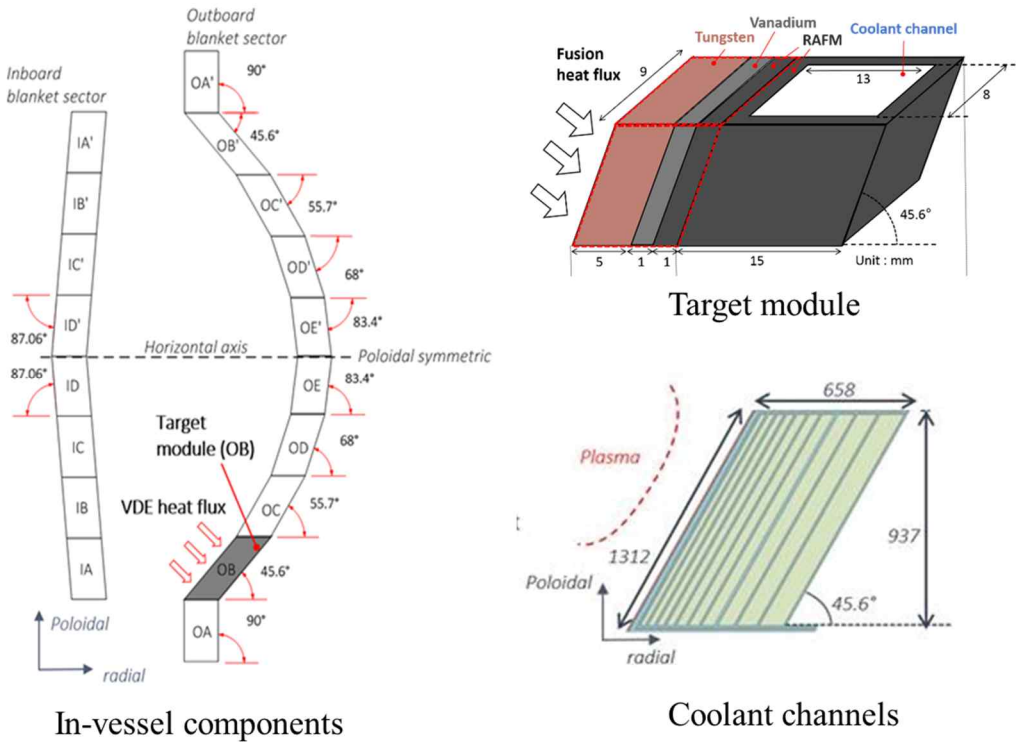

Figure 3.1 Blanket OB module in K-DEMO : VDE simulation target first wall

3.1.2 Code coupling between the phase change simulation module and MARS-KS

In order to simulate the thermal behavior of the first wall considering the heat transfer to the coolant channels, the target blanket OB module was nodalized as illustrated in Figure 3.2. There exist 12 pipes for the cooling channels tilted at 45.6° like a parallelogram shape, one of which very next to the target wall flows downward. The inlet header and the outlet headers are connected to the channels and between the pipes, heat structures were modeled.

Figure 3.3 shows the code coupling methodology of the first wall phase change simulation module and MARS-KS. The first three-layer of a target wall, tungsten, vanadium and the half-width of RAFM were simulated by phase change simulation module and the rest of the first wall, another half of RAFM and the other cooling channels were simulated by MARS-KS. The code interface was formed at the interior of the solid wall, RAFM layer.

Code coupling was conducted in an explicit method. First, the phase change simulation module calculated the one-dimensional heat conduction equation with implemented melting and evaporation model as described in Chapter 2. From the phase change simulation module, the temperature of the interface wall of RAFM was transferred to the MARS-KS boundary condition. At this time, the dynamic linked library version (DLL) of MARS-KS and the interactive control were used to receive wall temperature at the code interface. At the same time step, MARS-KS calculated the other parts and transferred the temperature of the code interface wall and the first cell.

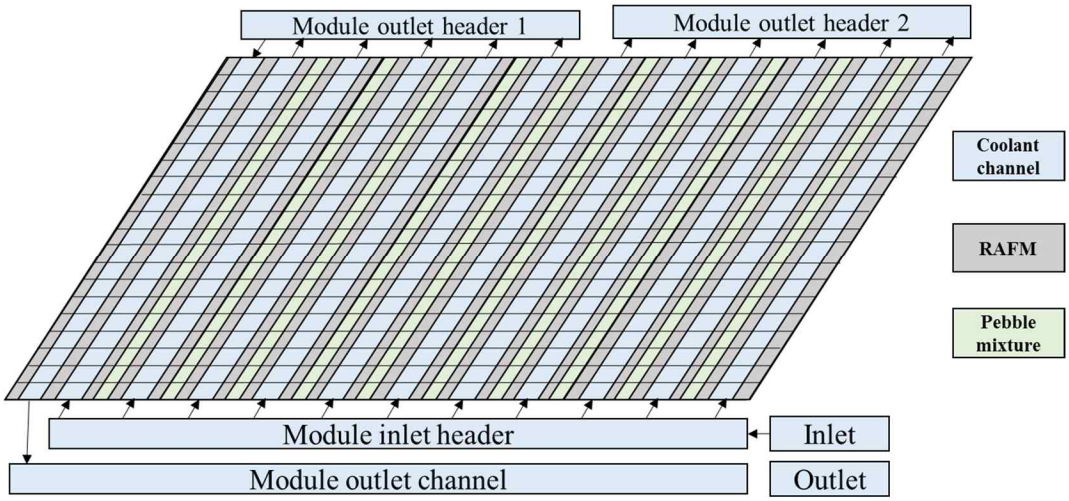

Figure 3.2 MARS nodalization of target blanket cooling system

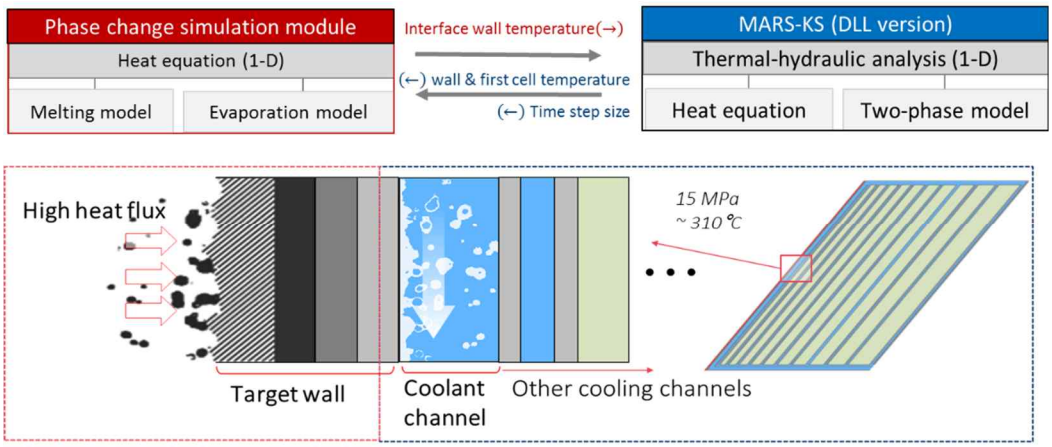

Figure 3.3 Code coupling of first wall phase change module and MARS-KS

3.1.3 Simulation results under various VDE cases

The melting, evaporation, and re-solidification of the first wall under 5 different VDE cases were simulated. The sequence of first wall phase change is illustrated in Figure 3.4. After the onset of the VDE, due to the impact of the high heat flux on the solid surface, the temperature of the structure rapidly increases. The maximum temperature of the plasma facing surface shown in Figure 3.5 exceeded the melting point and continuously increased. The melting of the first wall occurred and the melting front, which is the position of the liquid-solid interface, penetrated the wall. Simultaneously with the melting progress, the evaporation of the first wall appeared on the plasma facing surface during the VDE. After the end of the VDE heat influx, evaporation no longer occurs. Meanwhile, the melted layer of the first wall was recovered through the re-solidification process. Figures 3.5 and 3.6 show the plasma facing surface temperature and the phase change thickness in depth direction over time under several VDE cases, respectively.

From the perspective of the structural integrity of the first wall, there exist key factors to analyze the thermal behavior as follow; 1) evaporated thickness, 2) penetration depth, 3) phase change duration time and 4) starting time of the melting. The factors are marked in Figure 3.7, which shows the transient phase change thickness in depth direction over time. First, evaporated thickness refers to the amount of vapor that expands freely into the vacuum vessel and cannot be recovered. Second, the solid line shows the penetration depth, the position of the melting front. It can be defined as the sum of the evaporated and melted thickness. Deeper penetration through the first wall can reduce the integrity of the whole structure. In third, the fast starting point of melting can cause the mechanical

stress of the structure, due to the formation of high temperature gradient. Finally, a duration time of the phase change, which is from the beginning of melting to the end of re-solidification is marked in Figure 3.7. With the longer duration time of the phase change, the flow in the melted layer might occur caused by the momentum of plasma particles, buoyancy driven force, or Marangoni effects.

In this respect, the simulation results are summarized in Table 3.2 and Figure 3.8. During the VDE-I scenario with the highest heat flux for the shortest time duration, a large amount of tungsten evaporated into the vacuum vessel and 194 μm out of 5 mm tungsten layer does not recovered. Meanwhile, during the VDE-V scenario with the lower heat flux imposed for longer time, phase change, melting and re-solidification were continued for 0.37 second.

While the evaporation thickness decreases regularly as the heat flux decreases from VDE-I to VDE-V, and the phase change duration time increases as the VDE duration time increases, the melted thickness was not proportional to VDE heat flux or the duration time. Accordingly, the largest melted thickness was calculated under the VDE-IV case, and the total penetration depth was the deepest under the VDE-III case.

It can be explained with the combined effect of the vapor shielding in heat flux and the phase change duration time. Figure 3.9 (a) and (b) show the energy consumed in evaporation and the heat influx to the first wall surface over time, respectively. In the case of the higher heat flux, the energy consumed for material evaporation increases. It acts as a vapor shielding barrier to the surface heat flux, which reduces the ultimate heat influx to the tungsten wall. In particular, in VDE-I cases the heat influx to the first wall decreased 53 % at the end of the evaporation. VDE-V case shows only 85 % decrease in heat influx. Therefore, with higher heat

flux conditions, total energy transferred to the wall that can be used to the melting process becomes smaller. For the case with minimum vapor shielding, remained heat influx consistently stroke the tungsten surface for longer VDE duration time. The effect of vapor shielding is also seen in Figure 3.5. After the tungsten evaporation starts, an increasing rate of the plasma facing surface temperature decreases smoothly. The change of slope was at maximum for the VDE-I case.

On the other hand, the energy transferred to the wall per unit time affects the calculation results of melted thickness. The lower heat flux for a longer time, the smaller the energy imposed on the wall per unit time. The lower energy is easily transferred into the wall according to the heat conduction, and the smaller portion is consumed as a latent heat for melting so that the melted thickness can become thinner. For these reasons, the maximum penetration depth and melted thickness were the highest under VDE-III and IV cases which have not been the target scenario in previous ITER simulations.

Table 3.2 Summary of simulation results

Cases	I	II	III	IV	V
Disruption time [sec]	0.1	0.15	0.2	0.25	0.3
Heat flux [MW/m^2]	600	400	300	240	200
Simulation results					
Evaporated thickness [μm]	194	126	78	44	22
Melted thickness [μm]	774	890	948	957	923
Penetration depth [μm]	968	1016	1026	1001	945
Phase change duration time [sec]	0.2	0.25	0.31	0.35	0.37
Phase change starting time [ms]	0.007	0.016	0.029	0.046	0.066

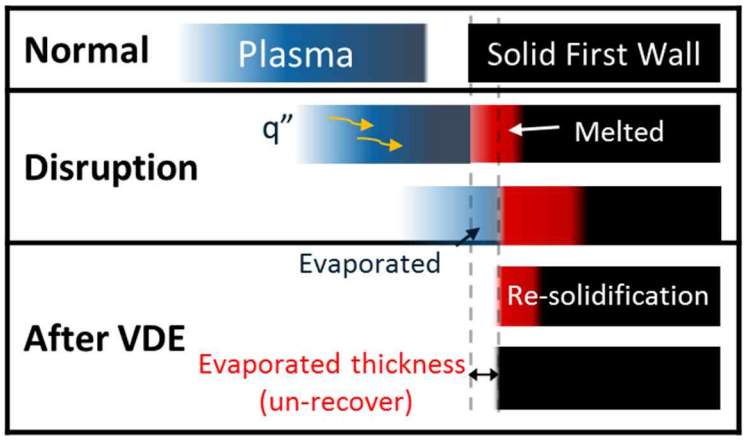

Figure 3.4 First wall phase change sequence

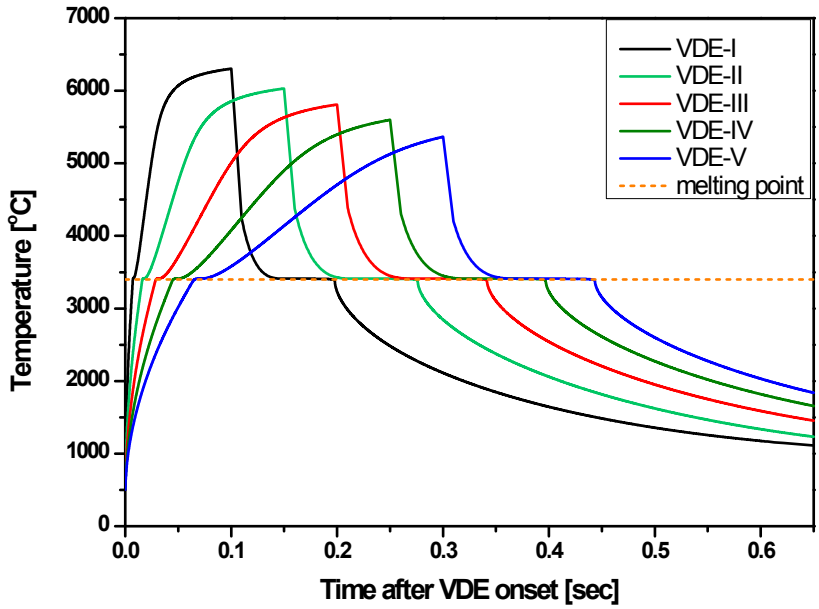

Figure 3.5 Plasma facing surface temperature

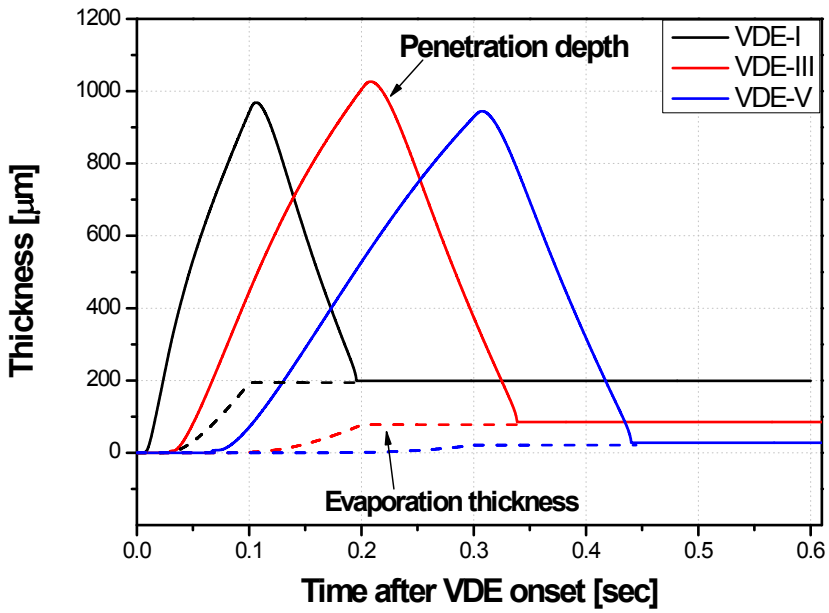

Figure 3.6 Phase change thickness transient result

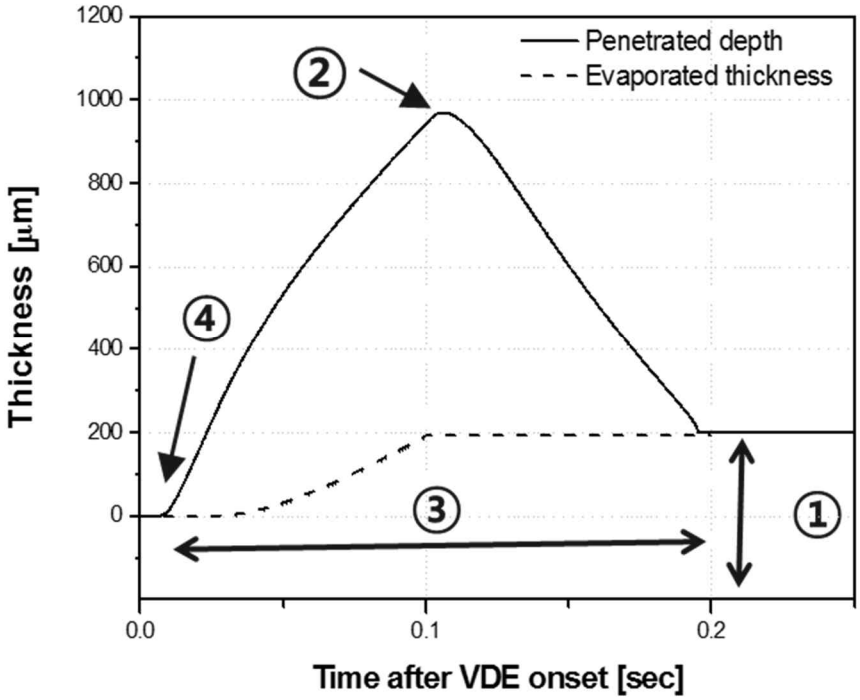

Figure 3.7 Key factors in the phase change simulation

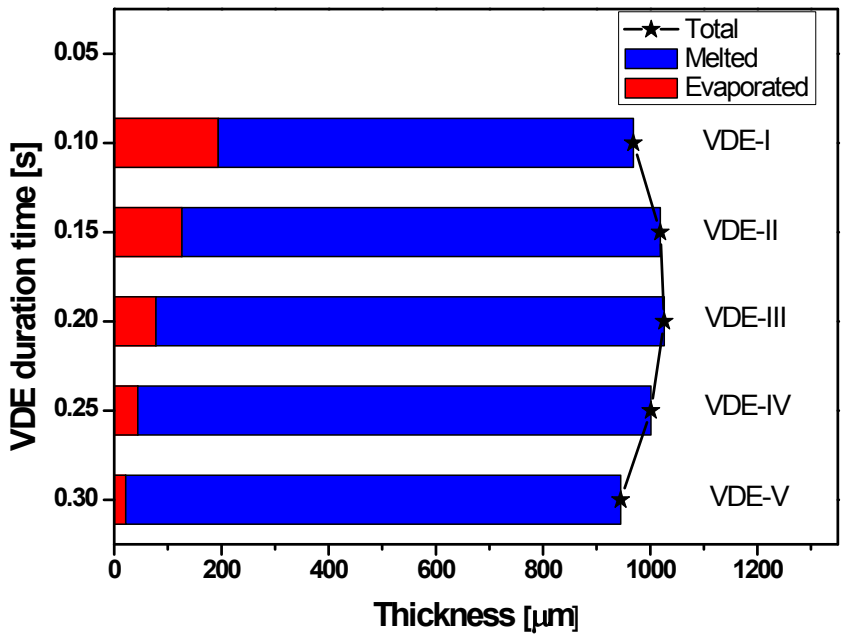

Figure 3.8 Phase change thickness in VDE cases

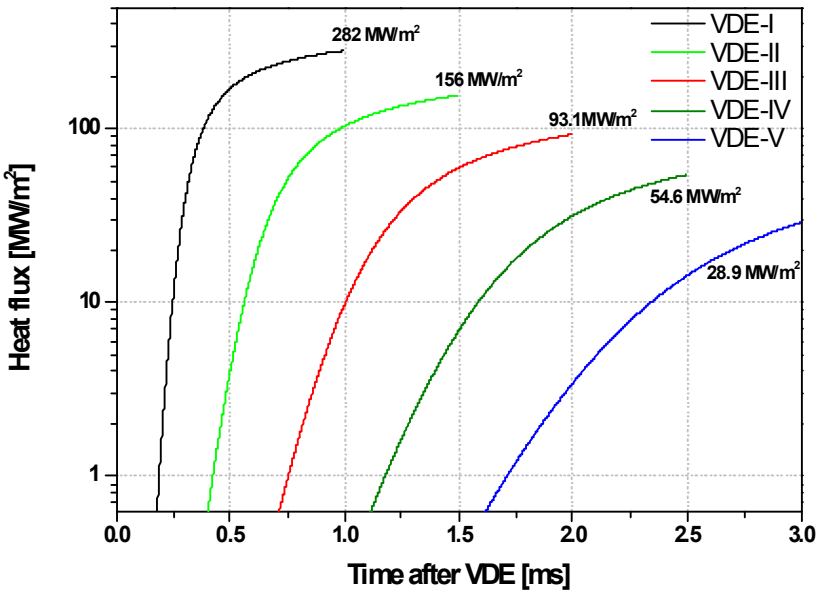

(a) Heat flux consumed in evaporation

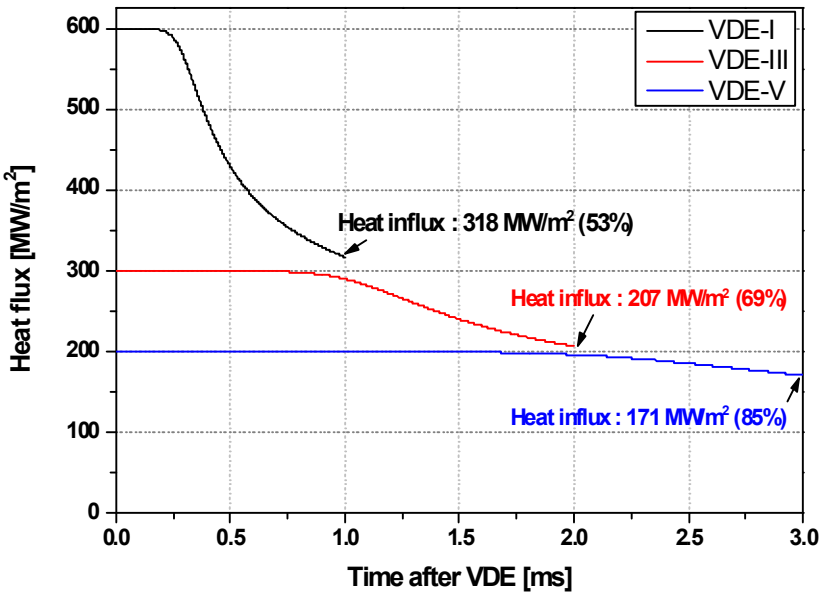

(b) Heat influx to the surface

Figure 3.9 Heat flux shielding with the evaporation

3.2 Effectiveness of the mesh adaptation

In this section, in order to identify the achieved effectiveness in the improved one-dimensional phase change simulation module with mesh adaptation technique, sensitivity tests were conducted under VDE-I scenario. The problem conditions are the same as in Table 3.1 and calculations with a various number of total meshes and mushy zone size were conducted with the two different mesh generation methodologies, uniform or adapted meshes. The mesh adaptation was applied only to the tungsten domain.

3.2.1 Grid sensitivity test and calculation efficiency

The element size analysis for VDE-I case with and without evaporation model was performed. The grid sensitivity and the convergences were tested by reducing the size of meshes in the tungsten domain. The mushy zone temperature range (10 K) and time step size, the meshes used for the vanadium and RAFM domain were fixed. The maximum of the melted and evaporated thickness and the position of the melting front were chosen as the parameters for comparison.

Firstly, the comparison results in melting simulation without the evaporation model are shown in Figures 3.10 and 3.11 in order to confirm the effect from r-refinement mesh adaptation technique. Other comparison results for the grid sensitivity test for lastly improved phase change module involving both melting and evaporation model were shown in Figures 3.12 and 3.13. As shown in Figure 3.10 and Figure 3.12, with the 500 meshes in total, the evaporated thickness and the penetrated thickness were converged and the phase change process was

precisely predicted. Different from this, by using the same number of meshes in a uniformly fixed system, the phase change behavior of tungsten was not simulated correctly and its phase change thickness was over-predicted.

As shown in Figure 3.11, with the uniform meshes, the maximum melted thickness on melting simulation was not converged during the tests. That is because of the limitation of EHCM described in Chapter 2. There are two different main reasons; the number of cells skipped over during the propagation of the melting front and the large size of cells. The minimum 1 μm length mesh from the 5000 meshes in 5 mm tungsten layer, and time step size with 0.0001 second were not sufficiently small to properly calculate the specific latent heat. The temperature difference between adjacent cells becomes greater than the mushy zone range 10 K in one time step. It makes the melting front propagate into the wall with a higher speed stepping over some cells under the uniformly distributed cell domain. Although the increasing trend of the maximum melted thickness with the smaller number of meshes was observed in mesh adaptation technique, the simulated results converged faster with a small number of meshes, using the mesh adaptation technique.

The results of grid sensitivity tests for the melting and evaporation simulation have the same tendency. Under the 3 K and 10 K mushy zone range, the grid sensitivity tests were conducted. Test results converged faster with the phase change simulation module improved with the mesh adaptation technique than the module using the uniform meshes. The effect of the implementation of the mesh adaptation compared with the uniform mesh is clearly shown under the smaller mushy zone range, 3 K. From 400 to 5000 meshes in total, the whole test results were converged, while the results from the uniformly fixed 5000 meshes were not

converged yet.

Resultantly, the implementation of mesh adaptation has its advantage that it can reduce the calculation time for the first wall phase change simulation. Depending on the test results shown in Figure 3.13 (a), the one-dimensional phase change simulation module with mesh adaptation technique accurately simulated the phenomenon in 113 minutes with the 400 meshes, while the module with 5000 uniform mesh system calculated in 533 minutes with low accuracy. The improvement of phase change simulation module speeds up to 5 times faster with the mushy zone range of 3 K.

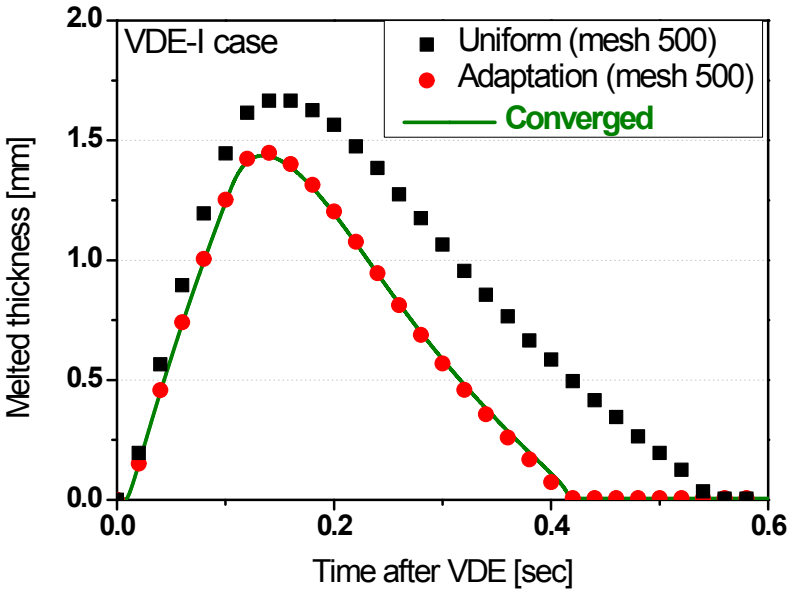

Figure 3.10 Comparison result on melted thickness

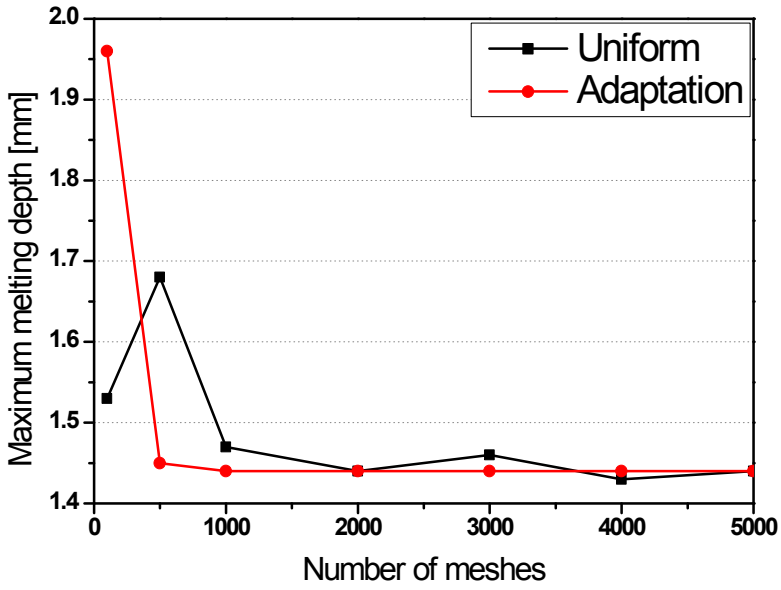

Figure 3.11 Grid sensitivity test results in melting simulation

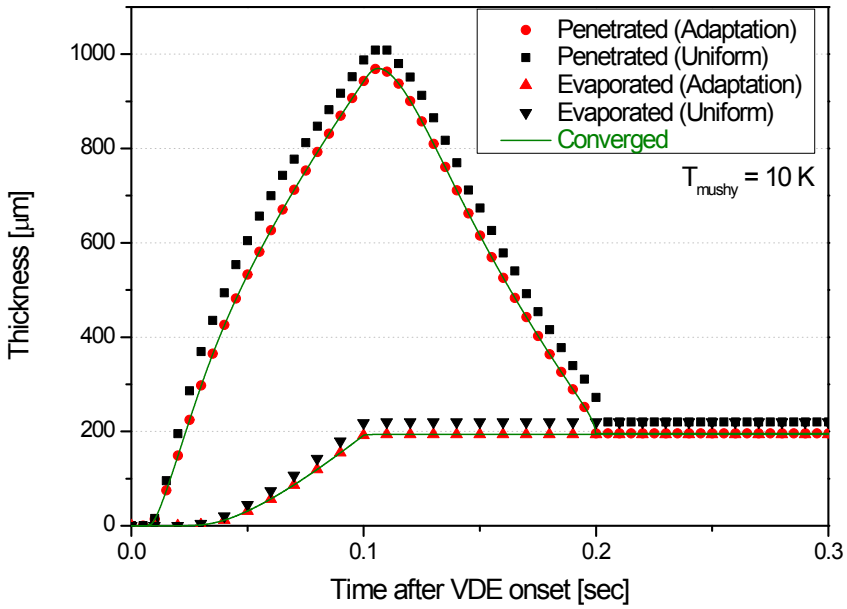

Figure 3.12 Comparison result on phase change thickness

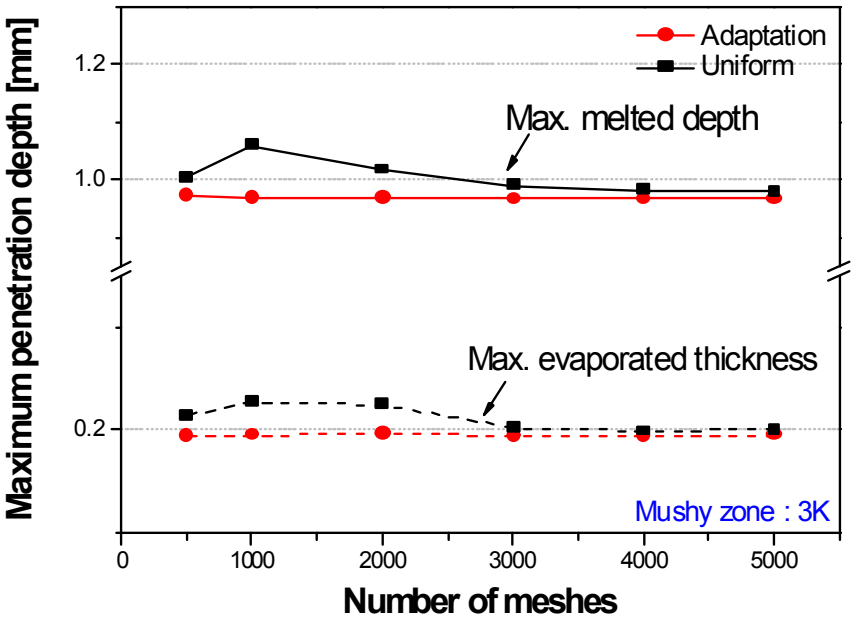

(a) Mushy zone: 3 K

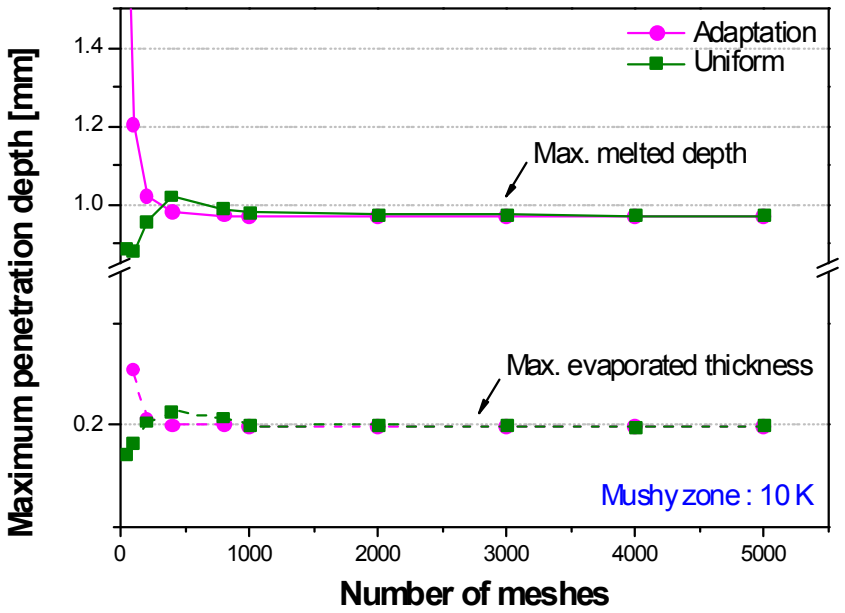

(b) Mushy zone: 10 K

Figure 3.13 Grid sensitivity test results with different mushy zone size

3.2.2 Mushy zone size dependency

The sensitivity test under VDE-I melting simulation was performed varying the mushy zone size and the total number of meshes in the tungsten domain. The mushy zone dependency was tested by increasing the total number of meshes in the tungsten layer, and the size of the mushy zone10 K. Figure 3.14 shows the sensitivity test results of uniform mesh methodology and adaptive mesh methodology. For the uniformly distributed meshes, most of the calculations failed to converge and a large number of meshes were required under every mushy zone ranges. In particular, for 1 K size of the mushy zone, it cannot achieve converged results with any size of uniform meshes. Furthermore, the number of meshes required to achieve convergence were greatly affected by the mushy zone size.

On the other hand, the simulation results converged by less than 1000 of adapted meshes under every condition. Moreover, it shows a very weak dependency for the mushy zone range. That is, regardless of the imaginary mushy zone range in the tungsten, sufficiently converged numerical melting simulation results can be obtained from improved one-dimensional phase change simulation module with the certain number of meshes.

In sum up, by using mesh adaptation technique in phase change simulation, independency to mushy zone size in convergence is achieved. The merits of the calculation module with mesh adaptation technique lead to the possibility of more realistic calculations. For the single component PCM, small mushy zone range can be selected so that the distortion caused by the virtual concept of the mushy zone can be reduced. The multi-component PCM such as improved alloy has its own mushy zone size. Independent to the size of its mushy zone, the convergence of phase change simulation can be ensured with mesh adaptation technique.

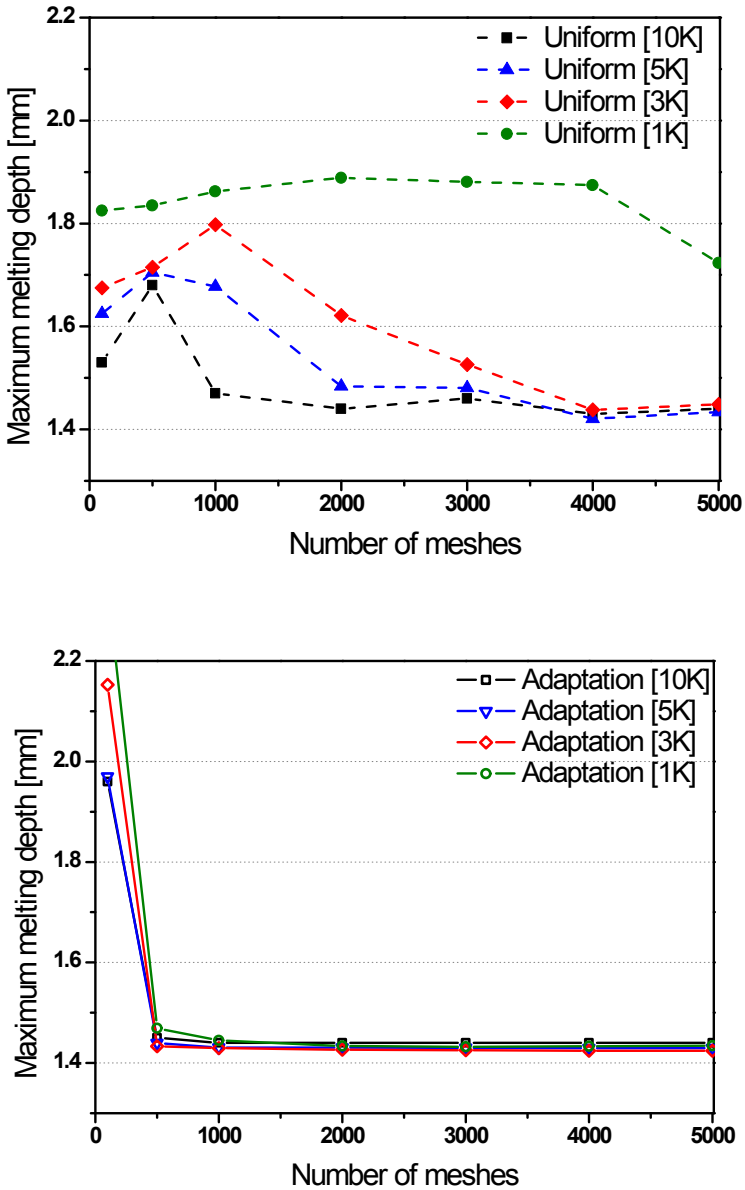

Figure 3.14 Mushy zone size and grid sensitivity test results
Uniform mesh method (top) Adaptive mesh method (bottom)

Chapter 4.

Phase Change Simulation with ANSYS-FLUENT coupled with MARS-KS

4.1 Multi-dimensional effect on melting simulation

4.1.1 Melting with convection heat transfer

In this chapter, the multi-dimensional effect on the melting of the structure under a high heat flux condition was analyzed. There exist forces within a melted layer that can cause an internal flow; natural convection induced by the buoyant force and the Marangoni effect caused by surface tension difference. In addition, in the nuclear fusion reactors, the momentum of plasma particles can be transferred to the plasma facing components (Schiller, 1988). The convective flow in the melted layer can change the shape of the liquid-vapor or liquid-solid interface and affect the heat transfer mechanisms. Kohei (2018) identified that Marangoni convection in the tungsten divertor can change the shape of a liquid-vapor interface. Moreover, the numerical and experimental studies on a natural convective heat transfer in the melted layer have been conducted for decades (Beckermann, 1988; Jany, 1988).

While the Marangoni effect occurs on the liquid-vapor surface, the natural

convection effect occurs within the melted pool as a whole and changes the heat transfer phenomenon in the depth direction of the wall. In this respect, the present study focused on identifying the effect of natural convection in the melted layer in the K-DEMO blanket.

The conceptual diagram of the convective heat transfer in the melted layer is illustrated in Figure 4.1. The heat transfer rate can be derived from a force balance between the buoyant force F_b and friction force F_f.

$$F_b = g\beta\Delta T \tag{4.1}$$

$$F_f = \frac{\nu v}{s^2} \tag{4.2}$$

where g, β, ν, ΔT, v, s are gravity, thermal expansion coefficient, kinetic viscosity, temperature difference through the melted layer, velocity in a melted layer, and the thickness of the melted layer.

The velocity in melted layer and total convective heat transfer rate can be derived as below:

$$v \sim \frac{g\beta\Delta T}{\nu} s^2 \tag{4.3}$$

$$Q_c \sim (\rho s v) c_p \Delta T \sim \rho c_p \frac{g\beta\Delta T^2}{\nu} s^3 \tag{4.4}$$

In general, because of the relatively high thermal energy in the top portion of the liquid phase part, more heat is transferred to the depth direction through the top so that the upper liquid-solid interface propagates deeper.

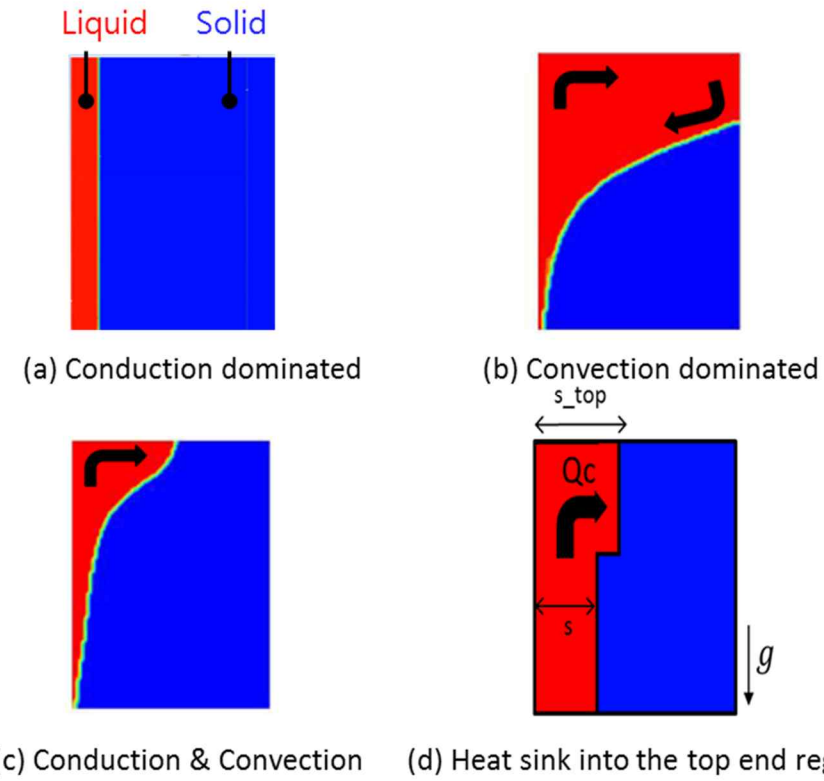

Figure 4.1 schematic diagram of liquid fraction in different heat transfer types

4.1.2 Non-uniform melting in K-DEMO first wall structure

The target first wall structure of K-DEMO is depicted in Figure 3.1 and the features were described in Chapter 3. Especially, the melting temperature of three different materials and the thickness of the structure are listed in Table 4.1. Tungsten has a high melting point and it is a component of the plasma facing structure with a thickness of 5 mm. The rest two materials have thinner structure thicknesses and lower melting temperatures than tungsten.

The non-uniform heat transfer rates at the top and bottom part lead to a temperature increase at specific sites. Then if the temperature of the top region increases locally with natural convection, the second and third layers can melt during the transient. Thus melting of the second and third layers at the first wall can yield safety concerns in the blanket phase change simulation. Figure 4.2 shows the examples of second and third layer melting behaviors in the first wall.

Table 4.1 Feature of the first wall layer

Feature	Tungsten	Vanadium	RAFM
melting temperature [℃]	3400	1910	1500
Thickness [mm]	5	1	0.5 (half)

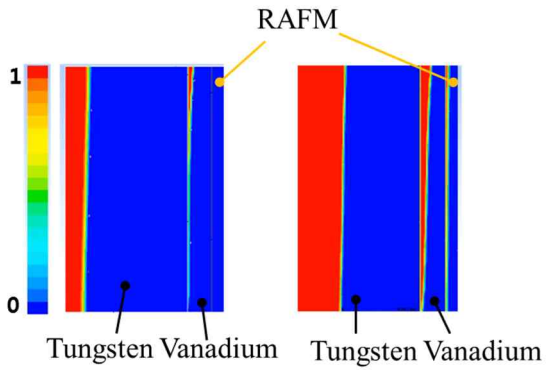

Figure 4.2 Examples of second and third layer melting (liquid fraction)

4.2 Coupled melting simulation between ANSYS-FLUENT and MARS-KS

In Chapter 3, though the one-dimensional phase change simulation module was improved and efficiently simulated the first wall phase change transient with the evaporation and melting models, the multi-dimensional analysis was conducted in this section. As the objective is to identify the convection heat transfer in the melted layer in a rapid transient coupled with a nuclear system analysis code, the evaporation that may occur on the plasma facing surface was not considered in the calculation. Multi-dimensional phase change simulation was conducted with ANSYS-FLUENT using its own melting model.

4.2.1 Melting model in FLUENT

The numerical model used in FLUENT for modeling the solidification and melting process is based on the enthalpy-porosity technique. This model solves the heat conduction equation in terms of enthalpy H, and treats the liquid to solid mushy zone as a porous zone to account for reduced porosity in the solid with a liquid fraction. The enthalpy increase in a mushy zone is calculated as the sum of the sensible enthalpy h, and the latent heat ΔH. The governing equation and the terms are defined as follows:

$$\frac{\partial}{\partial t}(\rho H) + \nabla \cdot (\rho v H) = \nabla \cdot (k \nabla T) + Q \tag{4.5}$$

$$H = h_{ref} + \int_{T_{ref}}^{T} C_p dT + \Delta H = h_{ref} + \int_{T_{ref}}^{T} C_p dT \beta L \tag{4.6}$$

$$\text{where,} \quad \text{liquid fraction } \beta \begin{cases} 0 & (T < T_{sol}) \\ 1 & (T > T_{liq}) \\ \dfrac{T - T_{sol}}{T_{liq} - T_{sol}} & (T_{sol} < T < T_{liq}) \end{cases} \tag{4.7}$$

Figure 4.3 shows the concept of the enthalpy-porosity technique. In an enthalpy-porosity technique, the liquid fraction is calculated at each iteration for every cell in the domain, based on an enthalpy balance. Referring to the FLUENT guideline, the model cannot be used for compressible flows and it cannot specify material properties separately for the solid and liquid materials. Therefore, in the present study, properties such as thermal conductivity and specific heat capacity were treated with table type. The property tables were used in the one-dimensional phase change simulation module before. In order to compare the melting model, code to code validation was conducted with present developed one-dimensional phase change simulation results using EHCM and that of ANSYS-FLUENT using enthalpy porosity technique. As shown in Figure 4.4, the calculation results from two different melting models matched within maximum 6.3 %.

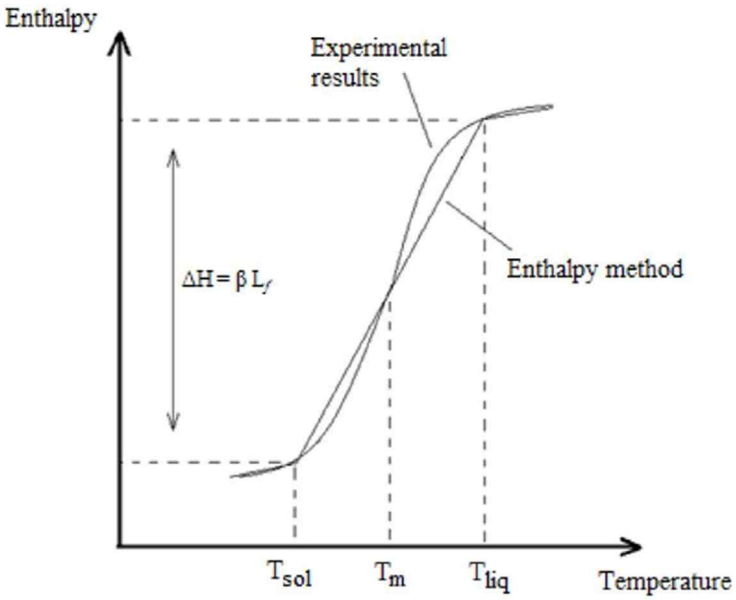

Figure 4.3 Concept of enthalpy porosity method

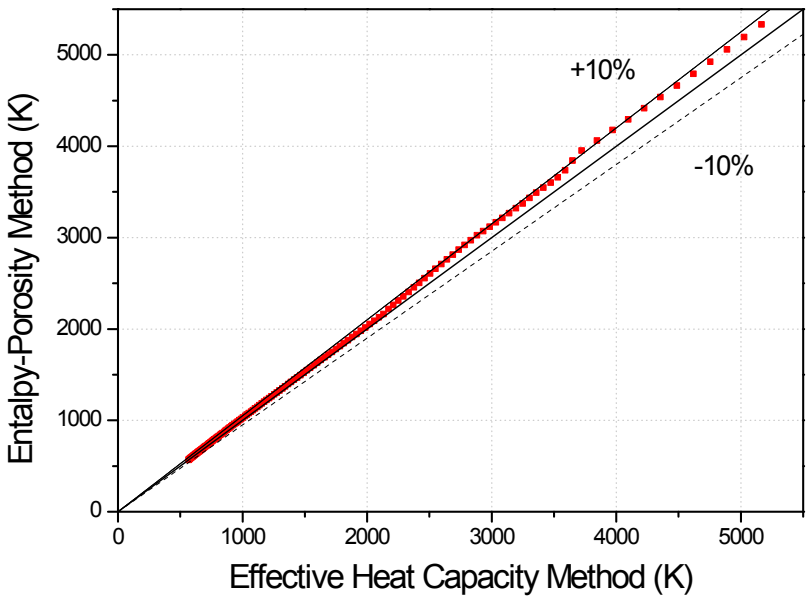

Figure 4.4 Comparison result of Enthalpy porosity method and EHCM

4.2.2 Code coupling between FLUENT and MARS-KS

Two-dimensional phase change simulation under a high heat flux condition was conducted with ANSYS-FLUENT coupled with MARS-KS. The target structure was selected to the first wall structure in the blanket OB module. Modeling of the first wall structure, 5 mm tungsten, 1 mm vanadium, and 0.5 mm RAFM layer was performed in FLUENT. Two types of first wall domain were modeled as shown in Figure 4.5. One is the 90° vertical wall in a rectangular shape, and the other domain was modeled in parallelogram shape, tilted to 45.6°. In the tungsten domain, 2000 x 200 meshes were generated. For the other parts, vanadium and RAFM, coarse meshes with 50 μm thickness were constructed. A 90° vertical domain was used to confirm the effect of natural convection in the melted region. And 45.6° tilted first wall domain is coupled with MARS-KS. For the plasma facing surface, 600 MW/m² were imposed as a high heat flux boundary condition, and the right-end wall consists of RAFM was coupled with MARS-KS or set as an isothermal boundary. The upper and lower boundaries were set as the adiabatic boundaries.

Same as the domain partitioned in one-dimensional phase change simulation in Chapter 3, the blanket OB module domain was divided into two parts as Figure 4.6. The nodalization for MARS-KS was the same as Fig. 3.2. At the code to code interface between FLUENT and MARS-KS, information of RAFM interior wall was exchanged. The time step size and the RAFM wall temperature are calculated in FLUENT and delivered to MARS-KS. At the same time, MARS-KS sends the heat flux information through the interface wall. The coupling was conducted explicitly.

Figure 4.7 shows the details in the code coupling methodology. CORBA

(Common Object Request Broker Architecture), socket communication, file I/O and user-defined function were used for the code coupling. Coupled calculations were conducted in the following process:

(1) Starting FLUENT from MATLAB
(2) Starting MARS-KS calculation
(3) Connecting the socket communication between each server and the client program
(4) File i/o from FLUENT at the end of time step
(5) Socket communication among MATLAB, Client, and MARS-KS
(6) File i/o from interface program

First of all, the MATLAB script controlled FLUENT running through the CORBA interface. During the whole simulation, boundary condition settings, variable extraction, and all calculation of FLUENT were controlled in the MATLAB script. The second step was to run MARS-KS waiting for the socket connection. Next, communication sockets are connected to each other. The MATLAB script and MARS-KS execute in independent servers and the interface code works as a client that communicates with each server. After the first calculation, the FLUENT extracts the time step and interface temperature in the form of a file. The MATLAB script receives that information and sends it to MARS-KS through a connected client socket. The temperature data delivered to MARS-KS is defined as the boundary condition. On the contrary, MARS-KS sends heat flux data as a control variable to the interface program, and the program writes the data in the form of a file readable by FLUENT.

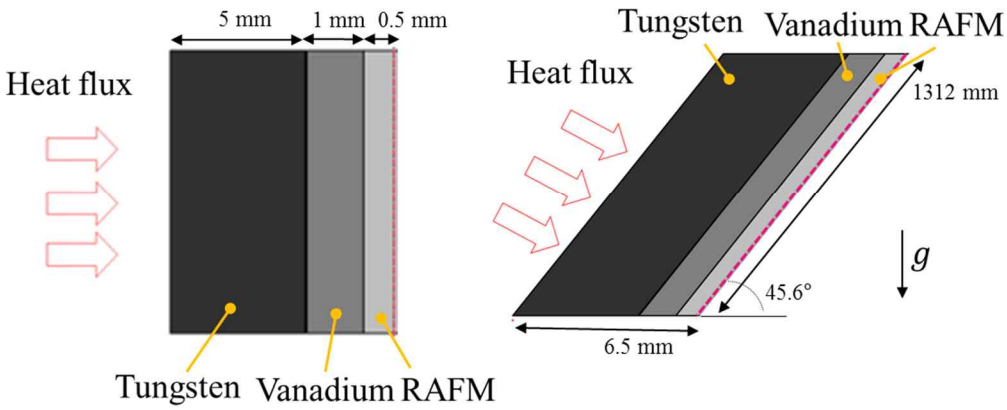

Figure 4.5 Modeling of first wall for two-dimensional simulation

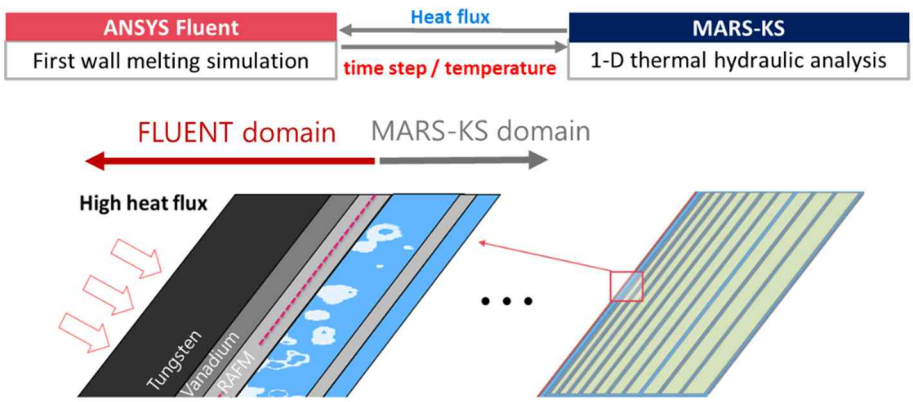

Figure 4.6 Modelling and domain partitioning in the coupled calculation

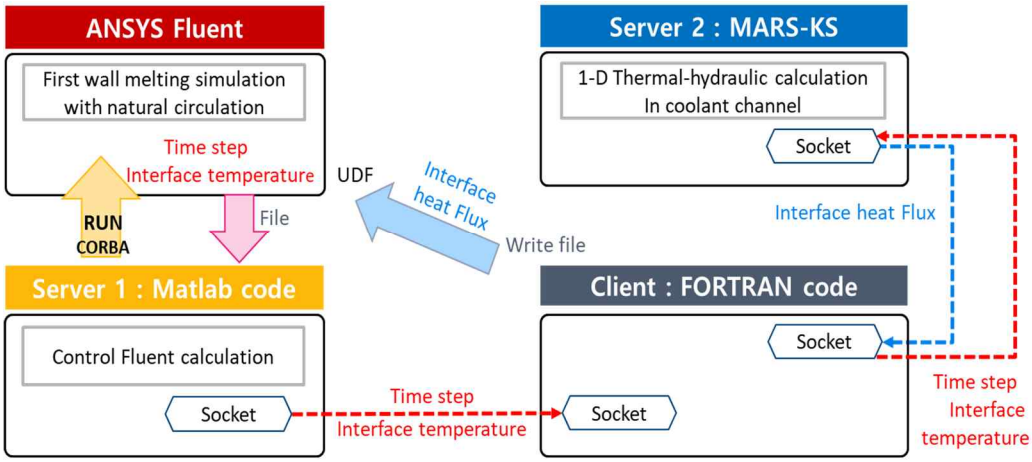

Figure 4.7 Code coupling methodology

4.2.3 Simulation results under the normal operation

Prior to the first wall melting simulation, verification of code coupling was conducted for normal operation. The conduction heat transfer equation through the blanket OB module was calculated with FLUENT and MARS-KS coupled method under the normal operation condition, listed in Table 3.1. During the normal operation, the imposed heat flux and plasma facing wall temperature are sufficiently low to avoid the solid phase change. For a verification purpose, the same simulation was conducted by MARS-KS that can simulate the whole part of the blanket OB module including first wall tungsten, vanadium, and RAFM layer. After the results reached a steady state, the temperature profile in the materials was compared between both methodologies. Figure 4.8 shows the comparison result of the MARS calculation and the FLUENT-MARS coupled calculation. As observed in Figure 4.8, the temperature distribution of the coupled code analysis is the same as that of the MARS-KS stand-alone analysis. From this results, it was concluded that the code coupling method was well established in FLUENT-MARS.

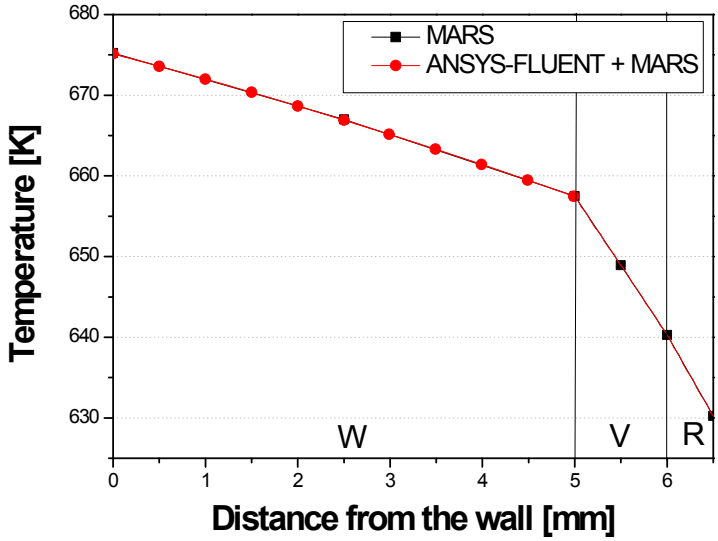

Figure 4.8 Coupled code verification result in normal operation

4.2.4 Simulation results of the transient scenario under high heat flux

Effect of natural convection in melting simulation with FLUENT

In order to identify the effect of natural convection in the FLUENT melting simulation, VDE-I simulations were performed with and without considering buoyant force and gravity. The tungsten part of the vertical first wall domain shown in Figure 4.5 was used. It was assumed that 600 MW/ m^2 heat flux was imposed to the plasma facing surface for 0.1 second, and the temperature of the right end, located on the opposite side was maintained at a constant temperature of 290℃. The results of melting simulations were depicted in Figure 4.9. Comparing the calculation results of FLUENT, the maximum difference in melted thickness is 0.23 mm. It is about 10 % of the maximum melted depth. When the natural convection effect in the melted layer was considered, moreover, the liquid–solid interface appeared inclined. As shown in Figure 4.10, the upper part in a tungsten domain melts deeper than the lower part, so that a slightly tilted mushy zone line was generated compared to the vertical line of the liquid-solid interface calculated without natural convection.

Coupled melting and re-solidification simulation under VDE

After investigating the natural convection effect in the melted layer, melting and re-solidification simulation for 45.6^o tilted first wall structure was conducted. As in the previous analysis, a heat flux of 600 MW/m^2 was applied for 0.1 second at the plasma facing surface. For the right end of RAFM wall, two different boundary conditions were imposed. First, the right end boundary acts as the code interface between FLUENT and MARS-KS, thus the heat flux through the RAFM

is calculated from MARS-KS and transferred to FLUENT. For the other case, the constant wall temperature was set to the right end boundary to simulate high efficient cooling conditions.

Figures 4.11-15 show the simulation results. As shown in Figures 4.11 and 4.13, during the melting simulation under VDE duration time (0.1 second), the propagation of the melting front in the tungsten appeared similar in two different RAFM boundary conditions. However, after the heat influx, a subcooled film boiling in the cooling channel occurs as a result of the system analysis with MARS-KS, and it reduces the cooling performance drastically. Therefore, the temperature rise in RAFM and coolant channels occur with DNB (Departure from nucleate boiling) as shown in Figure 4.12. Thus, both maximum melted thickness and phase change duration time, especially the time duration for tungsten re-solidification increased with boundary condition change. In addition, for the same reason as above, a more serious problem was observed for a coupled case with reduced heat transfer efficiency. As depicted in Figures 4.14-15, the second and third layer melting was observed from the FLUENT and MARS-KS coupled calculation, while only the second layer vanadium melting appeared in FLUENT stand-alone calculation.

The results indicate the importance of cooling boundary conditions in the simulation of solid structure phase change under high heat flux conditions. In the rapid transient scenario under high heat flux conditions, the thermal-hydraulic characteristics such as flow regime in the cooling channels changed to affect heat transfer capability. It can affect the major safety factors in solid thermal behavior, such as phase change duration time and melted thickness. Therefore, to accurately simulate the heat transfer with structure phase change with ANSYS-FLUENT, the

consideration of thermal-hydraulic behavior in the whole cooling system connected to the structure and coupled calculation with nuclear safety analysis code are necessary. From a similar point of view, the limitation of nuclear safety analysis code that it cannot deal with material phase change simulation can be overcome by coupling with ANSYS-FLUENT.

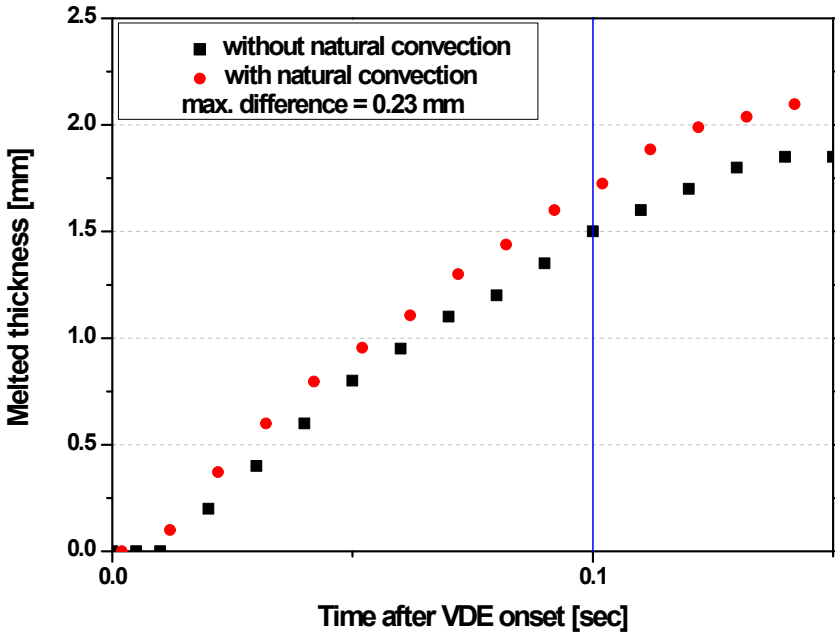

Figure 4.9 Propagation of melting front in tungsten domain

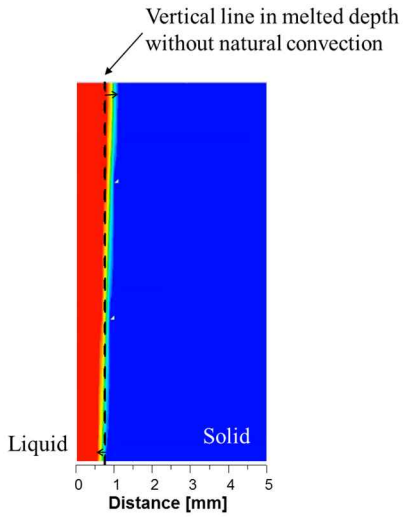

Figure 4.10 Liquid fraction in tungsten with natural convection

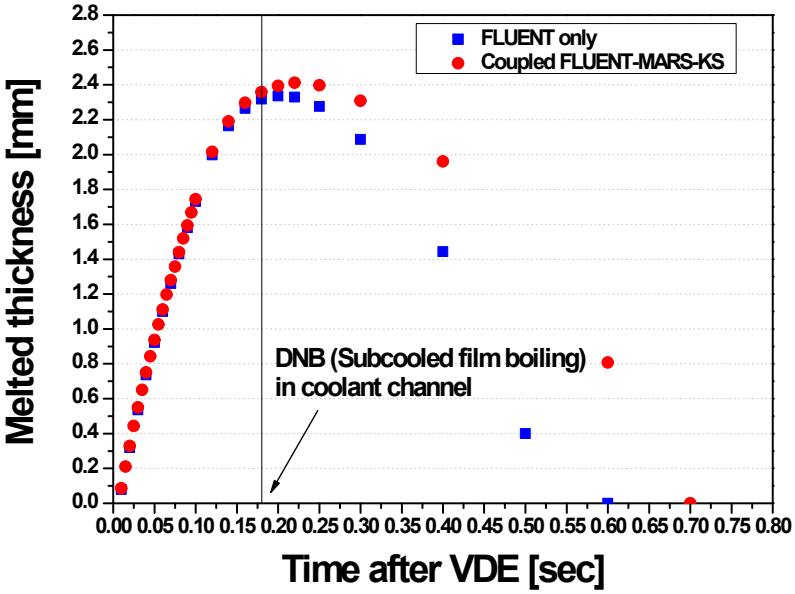

Figure 4.11 Melted thickness in tungsten layer

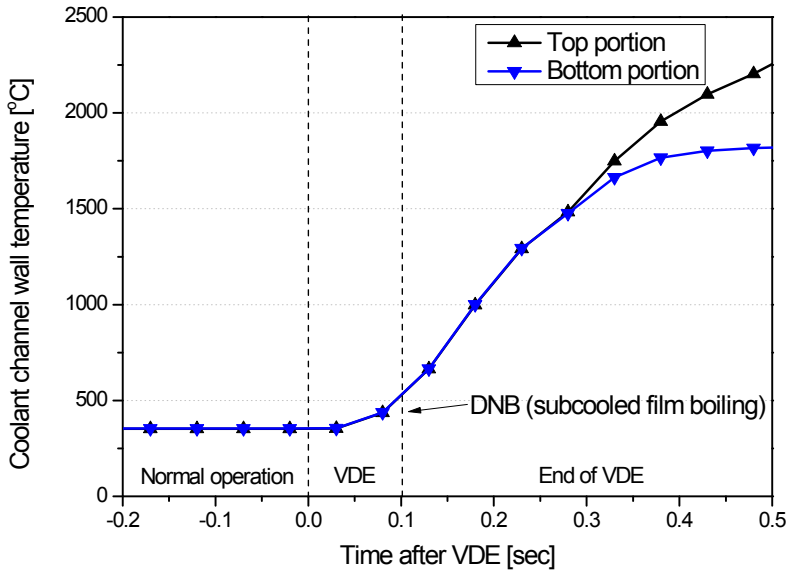

Figure 4.12 Coolant channel temperature

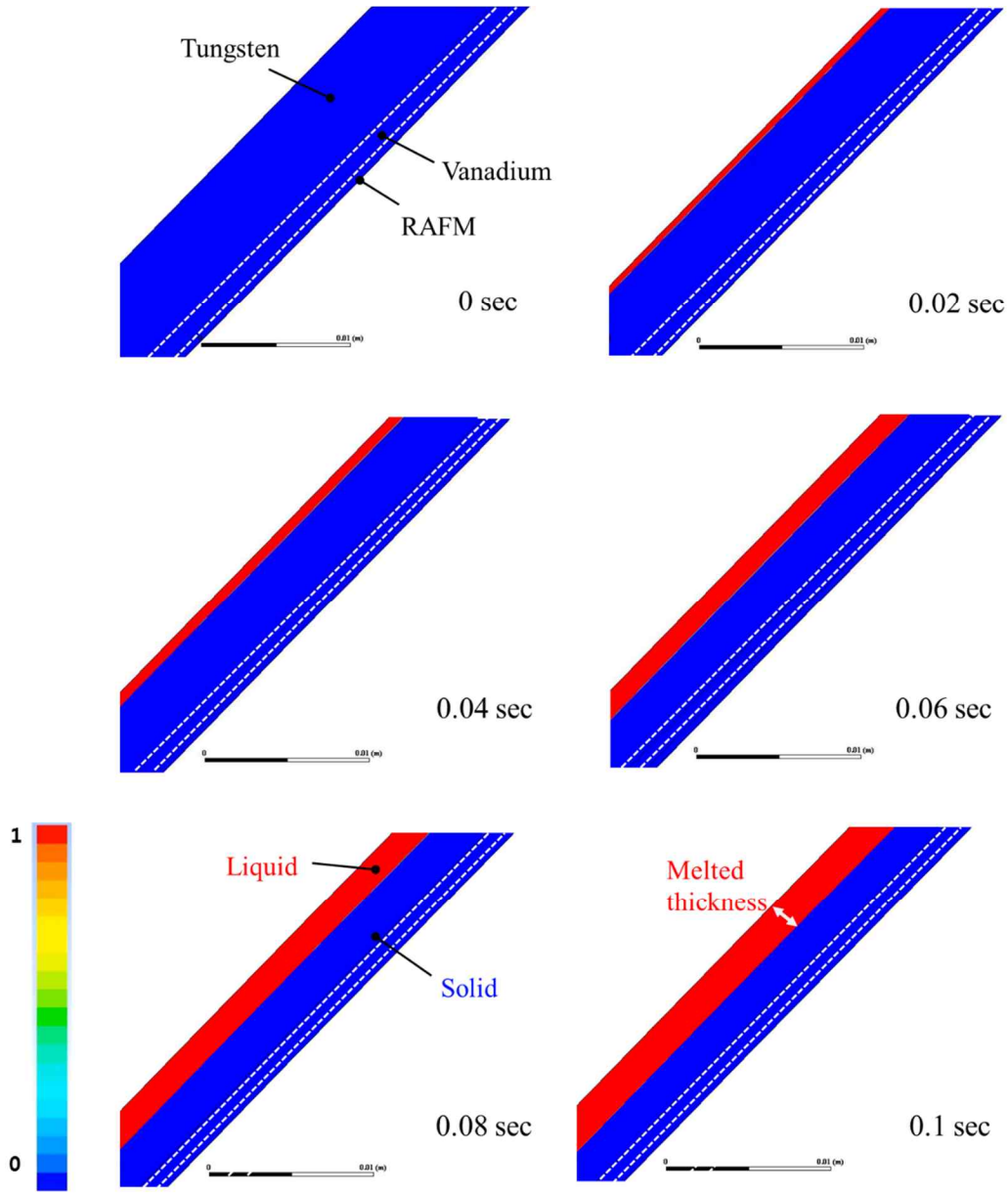

Figure 4.13 Propagation of melted layer during VDE-I

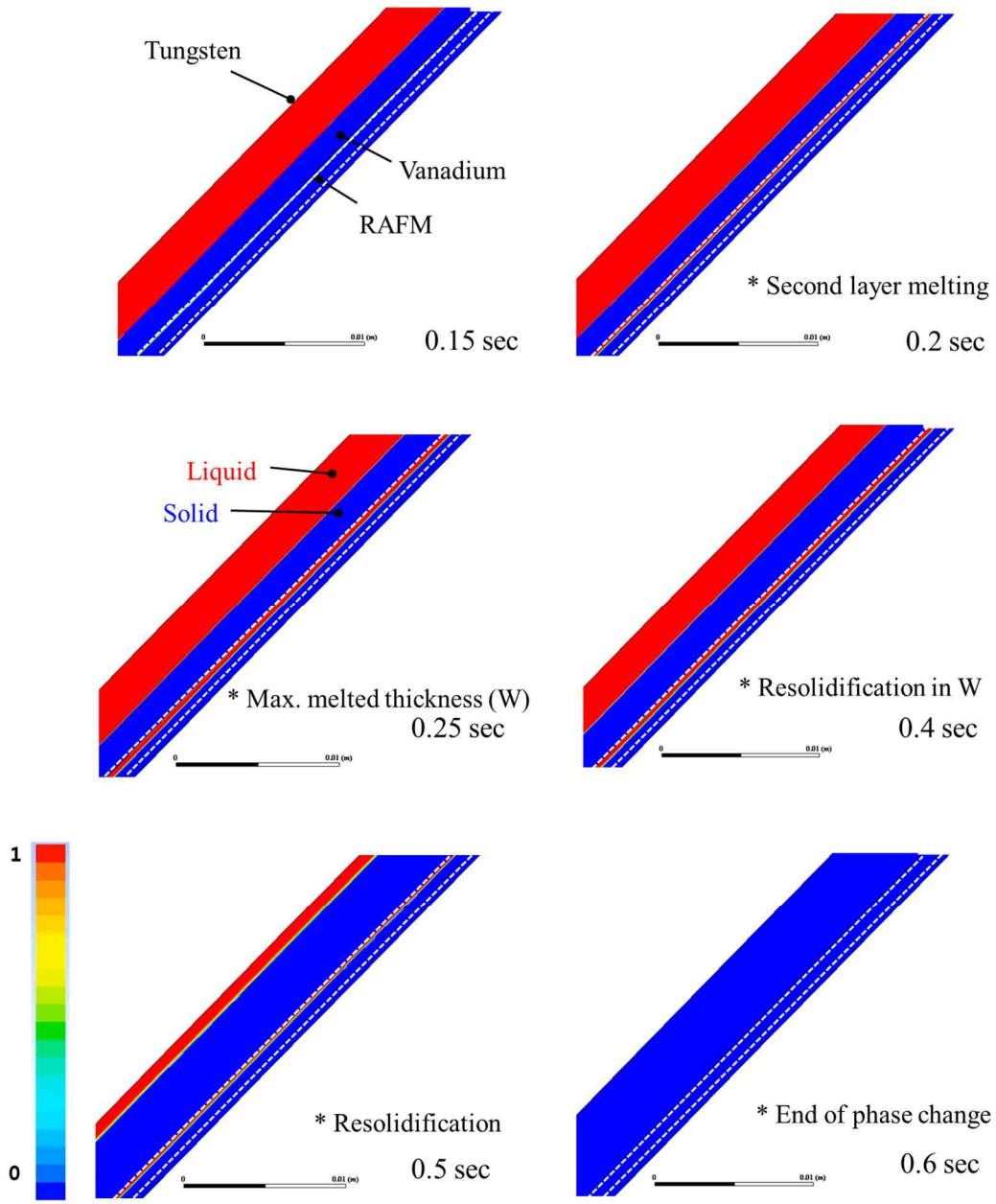

Figure 4.14 Second layer melting and re-solidification progress after VDE-I (FLUENT calculation)

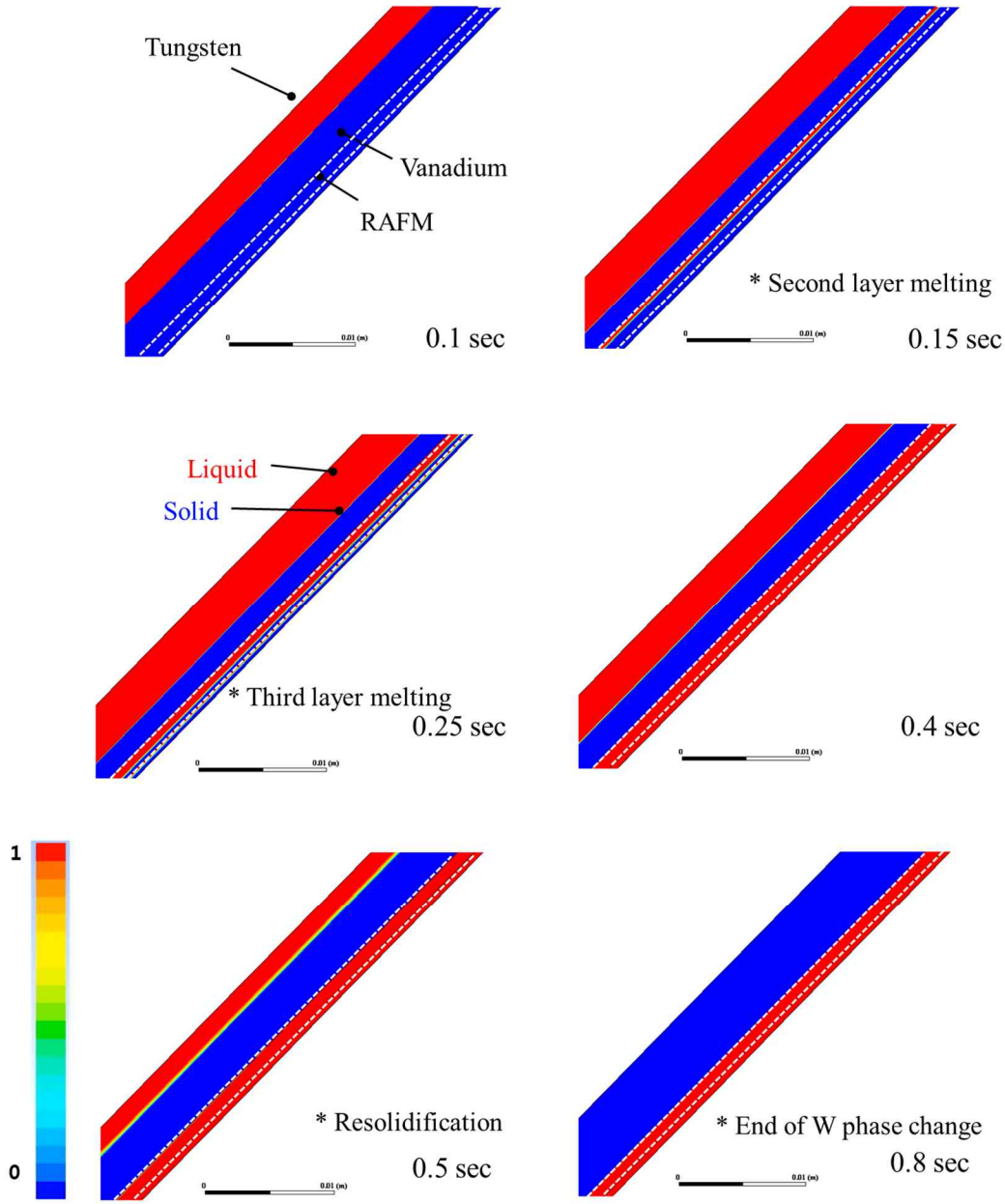

Figure 4.15 Second layer melting and re-solidification progress after VDE-I (FLUENT - MARS-KS coupled calculation)

Chapter 5.

Conclusion

5.1 Summary

In this thesis, the development of the one-dimensional phase change simulation module that can be coupled with MARS-KS was conducted. In addition, the calculation module was improved in efficiency and accuracy of the simulation by adopting the mesh adaptation technique using a monitoring function. With the module, thermal behavior analysis for K-DEMO blanket first wall was conducted in five different VDE cases. Afterwards, to identify the multi-dimensional effects during the melting of solid structure, the code coupling methodology between ANSYS-FLUENT and MARS-KS was established. Finally, the melting simulation under a high heat flux condition was performed. The results showed the natural convection effect in the melted layer and the two-phase flow heat transfer transition identified in the cooling system. The achievements of this study can be summarized as follows:

1. Improvement of the one-dimensional phase change simulation module

   The mesh adaptation technique shortened the calculation time by 5 times and reduced the mushy zone dependency in the convergence of the calculation. The improved module can be expected to simulate the more realistic phase

change efficiently for various solid materials.

2. Analysis of the tungsten phase change behavior under various VDE cases

   A Simulation was conducted for 5 different cases some of which were not covered by ITER's VDE simulation. It has been confirmed that one of the key factors in the structural thermal behavior, the total penetration thicknesses, were large in those cases.

3. Establishment of the code coupling methodology between ANSYS-FLUENT and MARS-KS

   The coupling methodology was established to identify the multi-dimensional effect of a natural convection in the nuclear system structure melting.

5.2 Recommendations

In this study, the one-dimensional phase change calculation module was improved by the mesh adaptation technique. Since the phase change calculations can be performed independent to the mushy zone size, it is expected that further calculations can be performed on various solid structures. In addition, because the present study was limited to the VDE transient simulation, the additional transient analysis such as electron run away in a tokamak reactor is required.

The multi-dimensional phase change simulation in this study predicted excessive temperature rise, because the material evaporation was not considered in ANSYS-FLUENT. For the further study, the multi-dimensional simulation considering the both melting and evaporation is suggested.

References

Beckermann, C., Viskanta, R., (1988) “Natural convection solid/liquid phase change in porous media,” Int.J. Heat and Mass Transfer, Vol. 31, pp. 35-46.

Cardella, A., Gorenflo, H., Lodato, A., et al, (2000) “Effects of plasma disruption events on ITER first wall materials,” J. Nuclear Materials, Vol. 283-287, pp. 1105-1110.

Hassanein, A.M., Kulcinski, G.L., Wolfer, W.G., (1984) “Surface melting and evaporation during disruptions in magnetic fusion reactors,” Nuclear Engineering and Design, Vol. 1, pp. 307-324.

Hassanein, A.M., Sizyuk, T., Ulrickson, M. , (2008) “Vertical displacement events: A serious concern in future ITER operation,” Fusion Engineering and Design, Vol.83, pp.1020-1024.

Hong, S.H., Kim, K., Kim, H. et al., (2018), “Damage and melting of ITER-like flat-type tungsten castellated blocks exposed to long pulse h-mode plasmas,” Fusion Engineering and Design, Vol.136, pp. 1518-1522.

Jany, P., Bejan, A., (1988), “Scaling theory of melting with natural convection in an enclosure,” Int. J. Heat and Mass Transfer, Vol. 31, pp. 1221-1235.

Kim, G.W., Cho, H.K., Park G.C., et al, (2017) “Melting and evaporation analysis of the first wall in a water-cooled breeding blanket module under vertical displacement event by using the MARS code,” Fusion Engineering and Design, Vol. 118, pp. 52-63.

Kim, K., Im, K., Kim, H.C. et al., (2015) “Design concept of K-DEMO for near-term implementation,” Nuclear Fusion, Vol. 55, 053027.

Kohei, H., Yu, T. Eiji, H. et al., (2018) “Development of a simulation method for evaluating Marangoni convection with free surface for tungsten divertor,” Fusion Engineering and Design, Vol. 136, pp. 270-275.

Komen, E.M.J., Koning, H., (1994) “Analysis of loss-of-coolant and loss-of-flow accidents in the first wall cooling system of NET/ITER,” J. Fusion Energy, Vol. 13, pp. 9-20.

Nakamura, M., Tobita, K., Someya, Y. et al., (2014) “Key aspects of the safety study of a water-cooled fusion DEMO reactor,” J. Plasma and Fusion research, Vol. 9, 1405139.

Nochetto, R.H., Siebert, K.G., Veeser, A., (2009) “Theory of adaptive finite element methods: an introduction, multiscale, nonlinear and adaptive approximation,” Multiscale, Nonlinear and Adaptive Approximation, pp. 409-542.

Ogoh, W., Groulx, D., (2010) “Stefan’s problem: Validation of a one-dimensional solid-liquid phase change heat transfer process,” Proceedings of the COMSOL Conference, Boston.

Ong, B., Russell, R., Ruuth, Steven., (2013) “An h-r moving mesh method for one-dimensional time-dependent PDEs,” Proceedings of the 21st international meshing roundtable, pp. 39-54.

Ozisik, M.N., (1968) “Boundary value problems of heat conduction,” International Textbook Co., Scranton, P.

Park, J.W, Song, H.J., (2017) “Numerical computation of a reactor vessel melting under external cooling conditions,” J. Nuclear Science and Technology, Vol. 54, pp. 694-704.

Schiller, P., Bross, F., Cambini, M. et al., (1988) “Experimental evidence for melt layer convection during disruption simulation experiments,” Fusion Engineering and Design, Vol. 6, pp. 131-136.

Welland, M.J., Lewis, B.J., Thompson, W.T., (2008) “A comparison of stefan and phase field modeling techniques for the simulation of melting nuclear fuel,” J. Nuclear Materials, Vol. 376, pp. 229-239.

국문초록

원자력 시스템 내에서 발생할 수 있는 고열속 과도 조건 하에서 여러 구조체는 그 열적, 구조적 건전성이 악화될 수 있다. 특히 고온의 플라즈마를 이용하는 핵융합로에서 플라즈마 대면재에 인가되는 고열속 조건은 구조체의 용융 및 증발 등 상변화를 유발한다. 또한 인가된 열속으로 인한 온도 상승은 냉각 채널의 소손(burnout) 상황을 야기하여 열전달 효율이 급격히 감소할 수 있다. 이 때 구조체 내에서 발생할 수 있는 상변화는 고체 내부를 포함하여 냉각 계통의 열전달 현상에 영향을 미친다. 따라서 고열속 조건 하에서 구조체의 상변화 열적 거동 분석과 막비등을 포함하는 냉각 계통의 2상 유동 열전달 거동 분석은 필수적이다. 하지만 지금까지의 안전성 연구는 각각의 단독 계산에 국한되어 있다. 이에 본 연구에서는 원자로 계통 열수력 코드와 연계하여 구조체의 상변화 열전달을 수치적으로 모사하는 것을 목표로 하였다.

먼저 구조체의 상변화를 포함한 열전달 모사를 위해서 1차원 열전도 방정식에 증발 및 용융 모델을 적용한 상변화 계산 모듈을 개발, 이용하였다. 이 때 용융 모델인 유효 열용량 기법이 가상의 머시영역을 이용함으로써 갖는 한계를 확인하였다. 이를 개선하기 위해 모니터링 함수를 이용하여 구조재 온도 변화에 따라 격자를 재구성하는 기법을 도입하였고, 계산 모듈의 효율성 및 활용도를 개선하였다. 모듈 개선을 통해 계산 시간을 5배 단축시켰으며, 보다 현실적인 구조체 용융 계산이 가능해졌다. 해당 1차원 상변화 계산 모듈은 DLL 버전의 MARS-KS 코

드와 연계하여, 구조체의 상변화와 냉각 계통을 포함한 고열속 과도 해석이 가능하도록 하였다.

핵융합 실증로 K-DEMO의 플라즈마 대면 구조체 중 하나인 블랑켓 1차벽을 대상으로 상변화 계산을 수행하였다. 플라즈마 불안정성에 의해 발생할 수 있는 VDE 상황을 열속의 크기와 인가 시간에 따라 5가지 케이스로 나누어 해석하였으며, 증발 두께, 용융 두께, 침투 깊이, 상변화 시작 시점과 지속 시간의 관점에서 구조체의 상변화 현상과 건전성을 분석하였다.

추가적으로, 다차원 용융물 내부에서 발생할 수 있는 자연 대류 효과를 확인하기 위해 ANSYS-FLUENT 를 이용한 2차원 용융 계산을 수행하였다. 그 결과 구조체 내부 유동은 고체와 용융물 경계의 형태 변화를 만들었다. 해당 계산은 소켓 통신을 활용하여 MARS-KS와 연계하여 냉각 계통의 거동과 함께 분석될 수 있도록 하였다. 연계에는 프로그램 간 제어 방식으로 CORBA를 사용하였으며, 소켓 통신과 파일 입출력 방식을 모두 활용하였다. 수립된 연계 방법론에 따라 블랑켓의 고열속 과도 상황을 해석하였으며, 냉각 채널 내 막비등 발생을 확인하였다. 또한 이로 인한 냉각 성능 저하, 용융 지속 시간 증가를 확인하였다. 실제 구조 건전성을 확인하기 위해서는 추가 증발 계산이 요구된다.

주요어: 고열속 과도해석, 고체 상변화 열전달, 머시 영역, 격자 재구성 기법, 블랑켓, MARS, FLUENT

학번: 2017-27568